

Accepted Manuscript

Influence of surface conductivity on the apparent zeta potential of TiO₂ nanoparticles: application to the modeling of their aggregation kinetics

Izzeddine Sameut Bouhaik, Philippe Leroy, Patrick Ollivier, Mohamed Azaroual, Lionel Mercury

PII: S0021-9797(13)00473-6
DOI: <http://dx.doi.org/10.1016/j.jcis.2013.05.034>
Reference: YJCIS 18819

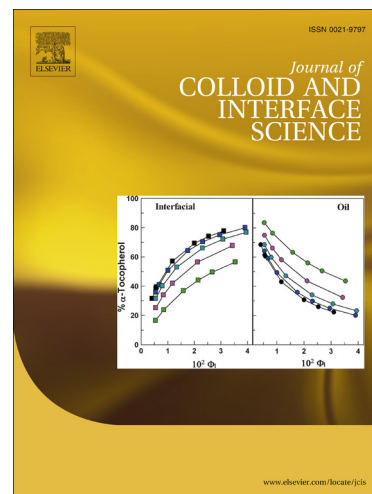
To appear in: *Journal of Colloid and Interface Science*

Received Date: 6 March 2013

Accepted Date: 15 May 2013

Please cite this article as: I.S. Bouhaik, P. Leroy, P. Ollivier, M. Azaroual, L. Mercury, Influence of surface conductivity on the apparent zeta potential of TiO₂ nanoparticles: application to the modeling of their aggregation kinetics, *Journal of Colloid and Interface Science* (2013), doi: <http://dx.doi.org/10.1016/j.jcis.2013.05.034>

This is a PDF file of an unedited manuscript that has been accepted for publication. As a service to our customers we are providing this early version of the manuscript. The manuscript will undergo copyediting, typesetting, and review of the resulting proof before it is published in its final form. Please note that during the production process errors may be discovered which could affect the content, and all legal disclaimers that apply to the journal pertain.



1 **Influence of surface conductivity on the apparent zeta potential of**
2 **TiO₂ nanoparticles: application to the modeling of their aggregation**
3 **kinetics**

4
5
6
7
8
9
10
11 5 Izzeddine Sameut Bouhaik^{1,2}, Philippe Leroy^{1*}, Patrick Ollivier¹, Mohamed Azaroual¹,
12
13 6 Lionel Mercury^{2,3}
14
15
16
17
18

19
20 9 ¹ BRGM, ISTO UMR 7327, 45060 Orléans, France

21
22 10 ² Université d'Orléans, ISTO UMR 7327, 45071 Orléans, France

23
24 11 ³ CNRS/INSU, ISTO UMR 7327, 45071 Orléans, France
25
26
27
28

29 13 * Corresponding author and mailing address:

30
31 14 Philippe Leroy

32
33 15 BRGM

34
35 16 3 Avenue Claude Guillemin

36
37 17 45060 Orléans Cedex 2, France

38
39 18 E-mail: p.leroy@brgm.fr

40
41 19 Tel: +33 (0)2 38 64 39 73

42
43 20 Fax: +33 (0)2 38 64 37 19
44
45
46
47
48
49
50
51

52
53
54
55
56
57
58
59
60
61
62
63
64
65

Intended for publication in *Journal of Colloid and Interface Science*

23 **Abstract**

24 Titanium dioxide nanoparticles (TiO₂ NPs) are extensively used in consumer products.
25 The release of these NPs into aquatic environments raises the question of their possible
26 risks to the environment and human health. The magnitude of the threat may depend on
27 whether TiO₂ NPs are aggregated or dispersed. Currently, limited information is
28 available on this subject. A new approach based on DLVO theory is proposed to
29 describe aggregation kinetics of TiO₂ NPs in aqueous dispersions. It has the advantage
30 of using zeta potentials directly calculated by an electrostatic surface complexation
31 model whose parameters are calibrated by ab-initio calculations, crystallographic
32 studies, potentiometric titration and electrophoretic mobility experiments. Indeed, the
33 conversion of electrophoretic mobility measurements into zeta potentials is very
34 complex for metal oxide nanoparticles. This is due to their very high surface electrical
35 conductivity associated with the electromigration of counter and co-ions in their
36 electrical double layer. Our model has only three adjustable parameters (the minimum
37 separation distance between NPs, the Hamaker constant, and the effective interaction
38 radius of the particle), and predicts very well the stability ratios of TiO₂ NPs measured
39 at different pH values and over a broad range of ionic strengths (KCl aqueous solution).
40 We found an effective interaction radius that is significantly smaller than the radius of
41 the aggregate and corresponds to the radius of surface crystallites or small clusters of
42 surface crystallites formed during synthesis of primary particles. Our results confirm
43 that DLVO theory is relevant to predict aggregation kinetics of TiO₂ NPs if the double
44 layer interaction energy is estimated accurately.

45 **Keywords:** stability ratio, TiO₂, nanoparticle, zeta potential, surface conductivity,
46 extended Stern model, linear superposition approximation, Derjaguin approximation,

47 surface element integration.

1
2
3
4
5
6
7
8
9
10
11
12
13
14
15
16
17
18
19
20
21
22
23
24
25
26
27
28
29
30
31
32
33
34
35
36
37
38
39
40
41
42
43
44
45
46
47
48
49
50
51
52
53
54
55
56
57
58
59
60
61
62
63
64
65

48 1. Introduction

49 A number of studies have recently focused on the transport and fate of nanoparticles
50 (NPs) in porous media and their potential risk for the environment and human health [1-
51 5]. However, their transport is very difficult to predict due to their very high surface
52 reactivity and, notably, to their versatility between their aggregated and dispersed states.
53 Modeling their reactivity and mobility in an aqueous environment is, therefore,
54 challenging [3, 6, 7].

55 Titanium dioxide (TiO_2) NPs are used in many consumer products (e.g. catalysts,
56 paints, coatings, soaps, cosmetics, and sunscreens [7-9]) because they have a very high
57 specific surface area and a sorption capacity for ionic and nonionic species [10, 11].
58 Their application for soil remediation and water treatment shows great potential [12-
59 14]. Their increasing use inevitably leads to their entering various environmental
60 compartments and questions now arise concerning their mobility, fate and toxicity for
61 humans and the environment.

62 Aggregation and deposition in porous media are the major processes controlling TiO_2
63 NPs transport [15]. Both processes are highly dependent on interaction energies
64 between particles (aggregation), and between particles and the surrounding aquifer rock
65 (deposition on the collector) [2, 16, 17]. The interaction forces between NPs and
66 between the NPs and the collector are controlled by the intrinsic properties of NPs
67 (chemical composition, size, and shape [2]) and by the intrinsic properties of the rock
68 (chemical composition and surface roughness [16]). When immersed in an aqueous
69 electrolyte, NPs and rock develop a surface charge (associated with the hydroxylation of
70 their surface and specific ion adsorption) and an electrical double layer (EDL) to cancel
71 it. EDLs around particles having similar chemical composition and crystal structure

72 have the same polarity and strength. As a result, when two particles draw near each
73 other, the overlapping double layers create a repulsive double layer force. This double
74 layer force between NPs (of similar chemical composition and crystal structure) and
75 rock can be repulsive if the EDLs of both materials have the same polarity (which
76 fosters aggregation), or attractive if the EDLs have opposite polarity (which fosters
77 deposition) [6, 7, 17].

78 When NPs are repulsed from the rock surface, interaction energies between NPs greatly
79 influence their aggregation [17]. TiO₂ NPs aggregate under specific chemical conditions
80 (pH, ionic strength, the chemical nature of aqueous dissolved species) that reduce the
81 repulsive double layer interaction energy between particles [10, 11]. Aggregation of
82 TiO₂ NPs decreases their mobility in porous media and may even clog the porosity if
83 their concentration in water is high. It may therefore enhance their deposition [7, 17].
84 However, their deposition can be reversible. Large quantities of TiO₂ NPs can be
85 released into the environment if the pH of the pore water changes and moves away from
86 the pH_{PZC} of TiO₂ NPs (PZC is the point of zero charge) or if the ionic strength of the
87 pore water decreases to values below the critical coagulation concentration (CCC) [7,
88 16, 17]. It is, therefore, important to understand the aggregation of titanium dioxide NPs
89 in water as a function of pH and ionic strength.

90 The double layer interaction energy is usually estimated using zeta potential data
91 inferred from electrophoretic mobility measurements [10, 18]. However, because of
92 their excess of electrical charges at the solid/water interface and very high surface-to-
93 volume ratio, metal oxide NPs can have a very high surface electrical conductivity. This
94 is associated with the electromigration of electrical charges in the double layer around
95 the particle and is inversely proportional to the size of the particle [18-21]. Surface
96 conductivity significantly decreases the magnitude of the electrophoretic mobility of

1
2
3
4
5
6
7
8
9
10
11
12
13
14
15
16
17
18
19
20
21
22
23
24
25
26
27
28
29
30
31
32
33
34
35
36
37
38
39
40
41
42
43
44
45
46
47
48
49
50
51
52
53
54
55
56
57
58
59
60
61
62
63
64
65

97 suspended particles when it is similar to or higher than the electrical conductivity of
98 bulk water [18, 19], i.e. at low ionic strengths (typically lower than 10^{-1} M), and for pH
99 values distant from the pH_{PZC} of the particle [18]. Under these physicochemical
100 conditions, the intrinsic or true zeta potential of the NPs can be significantly
101 underestimated if the zeta potential is not corrected for the retardation effect due to
102 surface conductivity. Both the resulting repulsive interaction energy between double
103 layers of particles and their stability ratios can therefore be underestimated.

104 Leroy et al. [18] recently developed a surface conductivity model for TiO_2 NPs
105 immersed in a 1:1 aqueous electrolyte (KNO_3 , $NaNO_3$, $NaCl$). In their work, surface
106 conductivity of the Stern and diffuse layers are calculated by an electrostatic surface
107 complexation model. Their electrokinetic transport model takes into account the
108 retardation effect due to surface conductivity of elementary NPs on the electrophoretic
109 mobility of the aggregate. Leroy et al. [18] adjusted the parameters of their extended
110 Stern layer model (ESM) using both potentiometric titration and electrophoretic
111 mobility experiments. Their corrected zeta potentials appear to be at least double the
112 apparent zeta potentials estimated using the Smoluchowski equation. These authors also
113 showed that potentiometric titration and electrophoretic mobility measurements of TiO_2
114 NPs can be predicted without the use of the unrealistic assumption of the presence of a
115 stagnant diffuse layer at the TiO_2 /water interface [8, 9].

116 Snoswell et al. [22] and Liu et al. [10] used the DLVO theory (constant charge
117 approximation and linear superposition approximation, respectively) to correctly predict
118 measured stability ratios of TiO_2 NPs immersed in a 1:1 aqueous electrolyte solution
119 (KCl and $NaCl$, respectively). However, they used low apparent zeta potentials (not
120 corrected for surface conductivity) and therefore predict low repulsive double layer
121 interaction energy between particles. Snoswell et al. [22] found an unrealistically low

122 value of 2×10^{-20} J for the Hamaker constant of the $\text{TiO}_2\text{-H}_2\text{O-TiO}_2$ interface compared
123 to values reported in the literature, which are between 4×10^{-20} J [23] and 9.4×10^{-20} J
124 [24]. The predictions of Liu et al. [10] were only in quantitative agreement with the
125 measured stability ratios of anatase NPs, which have two different sizes (mean radius of
126 either 5 or 50 nm). The aggregation kinetics model of Liu et al. [10] underestimated
127 stability ratios at low ionic strengths (2×10^{-3} M and 7×10^{-3} M NaCl for particles with a
128 mean radius of 5 and 50 nm, respectively). Moreover, their measured stability ratios of
129 anatase particles with a mean radius of 50 nm were not representative of stability ratios
130 of pure TiO_2 NPs because their particles contained large quantities of impurities (silicon
131 and phosphorous).

132 We provide here an aggregation kinetics model based on the DLVO theory and
133 combined with a precise description of the electrochemical properties of the TiO_2
134 NPs/water interface (using an extended Stern model) that is valid regardless of the size
135 of the NPs [18, 25]. The aggregation kinetics model uses true zeta potentials calculated
136 directly by our electrostatic surface complexation model. The combined model is
137 presented and tested against the stability ratios of pure TiO_2 NPs reported by Snoswell
138 et al. [22] at different pH values and in a KCl solution.

140 **2. Theoretical background**

141 *2.1. Aggregation kinetics models*

142 In aggregating systems, the coagulation rate is usually expressed by the stability ratio,
143 W , which is the ratio of the fast kinetic constant, k_f , to the slow kinetic constant, k_s ,
144 [26]. The aggregation rate is rapid when all collisions result in aggregation in the
145 absence of energy barriers, and slow in the presence of any repulsive energy barrier

146 (unfavorable conditions) that restricts aggregation to the primary minimum. The
147 stability ratio of suspended particles in aqueous environments can be predicted using
148 various DLVO and non-DVLO theories. The classic DLVO theory applies to smooth
149 and spherical colloidal particles immersed in water [27, 28] through two types of
150 interaction energies. The first is generally repulsive, due to the overlapping of the
151 particles' EDLs and the second is attractive, due to London–van der Waals (VDW)
152 interactions. However, NP aggregates have a more complex stability ratio than that of
153 perfectly spherical and smooth colloidal particles, notably because of the discreteness of
154 the surface charge [29, 30], the arising of relaxation processes [31-33], the presence of
155 additional non-DLVO forces [34, 35], and the surface roughness of the particles [22,
156 36]. The classic DLVO theory frequently overestimates the experimental NP
157 aggregation and deposition rates, probably by overlooking this complexity related to
158 these well-known characteristics [22, 29, 37, 38].

159 Kallay et al. [39] combined an electrostatic surface complexation model (basic Stern
160 model, BSM) and an aggregation model based on the DLVO theory to predict the
161 stability ratios of anisotropic rutile particles (length of 170 ± 70 nm and width of $45 \pm$
162 10 nm) immersed in a 1:1 aqueous electrolyte (LiCl, KCl, CsCl). The parameters of
163 their BSM were calibrated by crystallographic studies, potentiometric titration and
164 electrophoretic mobility measurements. Their approach [39] allows direct estimation of
165 the electrical potential at the outer Helmholtz plane (OHP). However, these authors
166 used the constant potential assumption [40] to estimate interaction energies between
167 particles and a too-simple equation to predict stability ratios. Indeed, this equation
168 assumes that the stability ratio is approximately proportional to the exponential of the
169 scaled maximum interaction energy. Additionally, Kallay et al. [39] did not compare
170 their predictions to measured stability ratios.

171 Non-DLVO theories have recently been proposed to explain the weaker-than-expected
172 stability of NP aggregates [41, 42]. Kallay and Zalac [41] consider that small NPs
173 (radius < 5 nm) surrounded by a diffuse layer are similar to ions surrounded by their ion
174 clouds because their size is small compared to the thickness of the electric double layer.
175 In their aggregation kinetics model, therefore, NPs interact like two interacting ions
176 sharing a common ion cloud. However, their model is only valid for NPs whose size is a
177 few nanometers. Furthermore, their model, which assumes that NPs are like hydrated
178 ions, is not realistic because NPs are an assemblage of atoms and molecules. For
179 example, to explain rapid aggregation of NPs at high ionic strengths (typically $>10^{-2}$ M),
180 their aggregation kinetics model assumes that the magnitude of the repulsive surface
181 charge density of the diffuse layer decreases with the ionic strength. In fact, this is not
182 the case for TiO₂ NPs immersed in an 1:1 aqueous solution (like NaCl or KCl) because
183 the magnitude of their surface charge density (at the surface of the mineral) increases
184 with salinity and therefore the magnitude of the surface charge density of the diffuse
185 layer also increases with salinity to cancel it [8, 9]. Zhang et al. [42] developed an
186 aggregation kinetics model based on the Maxwell approach. These authors assume that
187 NP aggregation is controlled mainly by their random kinetic motion because of their
188 nanometric size. They consider that aggregation could occur exclusively among the
189 fraction of NPs with the minimum kinetic energy that exceeds the interaction energy
190 barrier. In their model, the dispersed NPs are assumed to be Brownian particles in dilute
191 systems. That may be true for elementary NPs with a low surface charge density, but
192 NPs are often present in the form of aggregates in environmental media and the metal
193 oxide NP like TiO₂ NP has a large energy barrier due to its high surface charge density
194 [8, 9, 18]. Moreover, this aggregation kinetics model [42], as opposed to aggregation

195 kinetics models based on the DLVO theory, needs an additional fitting parameter to
 196 account for the hydrodynamic damping effect.

197 According to the DLVO theory and for perikinetic aggregation (by diffusion), the
 198 stability ratio is defined by the following equation [43]:

$$W = \frac{k_f}{k_s} = \frac{\int_{\min(u_a)}^{\infty} \beta(u_a) \frac{e^{V_{\text{TOT}}(u_a)/k_b T}}{(u_a + 2)^2} du_a}{\int_{\min(u_a)}^{\infty} \beta(u_a) \frac{e^{V_{\text{VDW}}(u_a)/k_b T}}{(u_a + 2)^2} du_a}, \quad (1)$$

199 where $\beta(u_a)$ is the correction factor for the hydrodynamic resistance between two
 200 approaching particles having radii a_1 (m) and a_2 , $u_a = 2d/(a_1 + a_2)$, d is the surface-to-
 201 surface separation distance between the two particles (m), k_b is the Boltzmann constant
 202 (1.381×10^{-23} J K⁻¹), and T is the absolute temperature (K). The parameters V_{TOT} and
 203 V_{VDW} (in J) represent total and van der Waals interaction energies between the two
 204 particles, respectively. V_{TOT} is the sum of the attractive van der Waals interaction
 205 energy and the (generally) repulsive electrical double layer interaction energy, V_{EDL} .
 206 The sign and the strength of this double layer interaction energy are given by the surface
 207 electrical potential, commonly assumed to be the zeta potential (ζ) [19, 44]. The latter is
 208 therefore a key parameter for the estimation of NP aggregation kinetics and must be
 209 accurately calculated. This is the reason why, in section 3, the zeta potential is
 210 calculated by an electrostatic surface complexation model. The correction factor for
 211 hydrodynamic resistance is described by the following approximation [43]:

$$\beta(u_a) = \frac{6u_a^2 + 13u_a + 2}{6u_a^2 + 4u_a}. \quad (2)$$

212 According to the DLVO theory, Eq. (1) shows that the stability ratio of electrically
 213 charged and suspended particles is strongly controlled by interaction energies due to

214 VDW and EDL forces. Two different approaches can be used to estimate the interaction
 215 energies between two spherical particles from interaction energies per unit area between
 216 two infinite flat plates: the Derjaguin approximation (DA) and the surface element
 217 integration (SEI).

218

219 *2.2. Interaction energies*

220 *2.2.1. Interaction energies between two infinite flat plates*

221 The non-retarded van der Waals interaction energy per unit area (E_{VDW} ; J m^{-2}) between
 222 two infinite flat plates separated by a distance h is calculated according to the Hamaker
 223 approach [45] by:

$$E_{\text{VDW}}(h) = -\frac{A_{\text{H}}}{12\pi h^2}, \quad (3)$$

224 where A_{H} is the Hamaker constant (J) which includes the dielectric information for the
 225 particles and the surrounding medium. The attractive London-van der Waals force arises
 226 from the bulk material properties of the particles and is caused by dipolar fluctuation of
 227 the atoms. The strength of this force is independent of the chemical composition of
 228 water surrounding the particles, and it decreases very rapidly with the surface-surface
 229 separation distance [27].

230 There is, as yet, no universal theory describing double layer interaction energy when
 231 two particles collide because, in that case, there is an overlapping of the diffuse layers
 232 and the double layer is not in thermodynamic equilibrium [32, 33, 36]. Three different
 233 approaches can be used to analytically estimate EDL interaction energy per unit area:
 234 constant charge approximation (CCA) [46], constant potential approximation (CPA)
 235 [40] and linear superposition approximation (LSA) [47].

236 CCA considers that the surface charge density is, therefore, constant, as is the total
237 number of counter-ions between the surfaces as the particles draw closer [46, 48]. The
238 counter-ions concentration and the repulsive double layer pressure increase accordingly.
239 CPA, on the other hand, assumes that the concentration of counter-ions between the two
240 surfaces remains approximately constant and the surface charge density diminishes as
241 the surfaces come together [40, 48]. Therefore, repulsive double layer interaction
242 energies predicted by CCA are higher than those predicted by CPA. CCA and CPA are
243 based on the linear Poisson-Boltzmann equation. These two methods consider a Debye-
244 Hückel ionic atmosphere, i.e. that the electrical potential in the diffuse layer follows a
245 Debye-Hückel distribution. Consequently, the analytical equations used by these two
246 models (to estimate the double layer interaction energy per unit area) are accurate only
247 for low surface electrical potentials (magnitude $< k_b T / ze$, where e is the elementary
248 charge of 1.602×10^{-19} C and z is the valence of a binary symmetric electrolyte) [19, 44].
249 Furthermore, these two approximations may be regarded as extremes, with the “true”
250 situation lying somewhere in between [2, 37, 49].
251 LSA is a useful compromise between CCA and CPA [2, 16, 47] that gives intermediate
252 values for the double layer interaction energy per unit area [47, 49]. This theory is based
253 on the calculation of the electrical potentials of isolated spheres, which can be done
254 numerically. This means that LSA can be used for higher surface electrical potentials
255 than CCA and CPA. This also means that LSA is particularly relevant when particles
256 are far apart, i.e. in cases where $\kappa h \gg 1$ [50], κ being the inverse of the Debye length,
257 which corresponds to approximately half the total thickness of the diffuse layer of
258 isolated particles [44]. According to LSA, the double layer interaction energy per unit
259 area can be written as [51]:

$$E_{\text{EDL}}(h) = 32\varepsilon_0\varepsilon_r\kappa\left(\frac{k_bT}{ze}\right)^2 y_1 y_2 e^{-\kappa h}, \quad (4)$$

with

$$y_{1,2} = \tanh\left(\frac{ze\psi_{d1,2}}{4k_bT}\right), \quad (5)$$

where ε_0 is the dielectric permittivity of vacuum (8.85×10^{-12} F m⁻¹), ε_r is the relative dielectric permittivity of water ($\varepsilon_r \cong 78.3$ for bulk water at a pressure = 1 bar and a temperature $T = 298$ K), and ψ_d is the electrostatic potential at the head-end of the diffuse layer (in V), which corresponds to the outer Helmholtz plane (OHP). This electrostatic potential is called the surface electrical potential, commonly assumed to be equal to the zeta potential (ζ) [19, 44].

The inverse of the Debye length, κ , is calculated by :

$$\kappa = \sqrt{\frac{2000e^2 N_A I}{\varepsilon_0 \varepsilon_r k_b T}}, \quad (6)$$

$$I = 0.5 \sum_{i=1}^N z_i^2 c_i^b, \quad (7)$$

where N_A is the Avogadro number (6.022×10^{23} mol⁻¹), I is the ionic strength of the solution (mol dm⁻³), N is the number of types of ions in the bulk electrolyte (superscript “ b ”) of valence z_i , and concentration c_i (mol dm⁻³).

2.2.2. Derjaguin approximation and surface element integration

The Derjaguin approximation (DA) enables us to calculate the interaction energy, V , between two spherical surfaces from the interaction energy per unit area between two plane surfaces, E , according to [28]:

$$V_{DA}(d) \approx \int_A E(h) dA \approx \frac{2\pi a_1 a_2}{a_1 + a_2} \int_d^\infty E(h) dh, \quad (8)$$

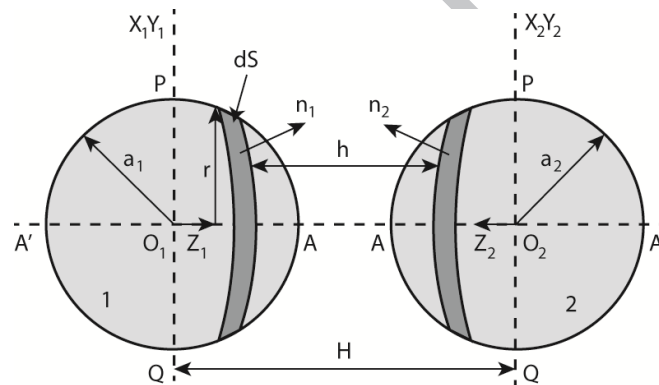
276 where d is the distance of closest approach between the two curved surfaces and A is the
 277 area of the facing surfaces. Equations for the calculation of the interaction energies are
 278 written in Appendix A.

279 The main assumption in the Derjaguin approximation is that the range of the interaction
 280 energy is much shorter than the radii of curvature of the particles. The function outside
 281 of the integral in Eq. (8) represents curvature effects that are valid only near the distance
 282 of closest approach, d . This means that DA is accurate if the distance between the two
 283 surfaces is much smaller than the shortest radius of the two particles, i.e. when
 284 $d \ll a_{\min}$ [52]. This also implies that DA is accurate for thin double layers relative to
 285 the smallest radius, i.e. when $\kappa a_{\min} > 10$ [51]. Furthermore, Derjaguin's technique
 286 considers that a surface element interacts with another element directly facing it with an
 287 intensity $E(h)$. This assumption becomes progressively inaccurate as the separation
 288 distance between particles increases. DA overestimates the interaction energy between
 289 two particles when the condition $d \ll a_{\min}$ is not satisfied [51-53]. To avoid the main
 290 assumptions of DA, we use a specific computing method, surface element integration
 291 (SEI), which discretizes the area over which the two surfaces interact.

292 The surface element integration method calculates the total interaction energy between
 293 two particles by numerically integrating the interaction energy per unit area between
 294 opposing differential planar elements over the entire surfaces. For two spherical
 295 particles and according to the SEI method, the interaction energy can be written as:

$$V_{SEI}(d) = \int_{S_1} dV = \int_{A_1} \mathbf{n}_2 \cdot \mathbf{k}_2 \frac{\mathbf{n}_1 \cdot \mathbf{k}_1}{|\mathbf{n}_1 \cdot \mathbf{k}_1|} E(h) dA_1. \quad (9)$$

296 In Eq. (9), the centers of particles 1 and 2 are origins of two body-fixed coordinate
 297 systems, with their z axes directly facing each other (Fig. 1). The xy planes of these
 298 coordinate systems are parallel to each other (see Bhattacharjee et al. [51] for more
 299 details relative to SEI). The parameter S_1 in Eq. (9) is the surface of particle 1, A_1 is the
 300 projected area of particle 1 on the xy plane, vectors \mathbf{n}_1 and \mathbf{n}_2 are the outward unit
 301 normal to the surfaces of the two particles, and vectors \mathbf{k}_1 and \mathbf{k}_2 are the unit vectors
 302 directed towards the positive z axes of each body-fixed coordinate system. The scalar
 303 products $\mathbf{n}_1 \cdot \mathbf{k}_1$ and $\mathbf{n}_2 \cdot \mathbf{k}_2$ can have both positive and negative values. Equations for
 304 the calculation of the interaction energies are written in Appendix A.



305
 306 **Fig. 1.** Two interacting spherical particles with radii a_1 and a_2 . The centers of the
 307 spheres are origins of two body-fixed coordinate systems, with their z axes directly
 308 facing each other. The xy planes of these coordinate systems are parallel to each other
 309 (from Bhattacharjee et al. [51]).

310
 311 According to Bhattacharjee et al. [51], SEI, on the contrary to DA, doesn't grossly
 312 overestimate the repulsive double layer interaction energy between particles (with the
 313 same radius a) when $\kappa a < 10$. This can be the case for NPs immersed in a dilute
 314 aqueous solution. Furthermore, Eqs. (8) and (9) are based on the assumption of pairwise
 315 interaction between two facing surface elements. The error involved in this assumption

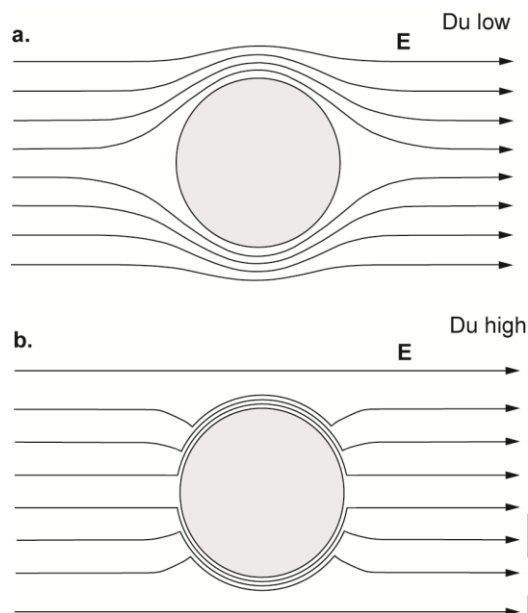
1
2
3
4
5
6
7
8
9
10
11
12
13
14
15
16
17
18
19
20
21
22
23
24
25
26
27
28
29
30
31
32
33
34
35
36
37
38
39
40
41
42
43
44
45
46
47
48
49
50
51
52
53
54
55
56
57
58
59
60
61
62
63
64
65

316 will be small only when the interaction energy is very short-ranged. These two
317 equations assume that the interaction force per unit area acts normal to the particle
318 surface, which is rigorous only for a constant surface potential [51].

319

320 *2.3. Zeta potential*

321 Snoswell et al. [22] used Henry equation [54] to convert electrophoretic mobility
322 measurements of TiO₂ nanoparticles into apparent zeta potentials. However, this
323 equation only considers the retardation effect associated with the size of the particle.
324 The conversion of electrophoretic mobility measurements of metal oxide NPs is very
325 difficult because these particles have an electrical double layer which affects the applied
326 electrical field around the particle [18] (Fig. 2). Surface conductivity is associated with
327 the electromigration of electrical charges in the double layer around the particle and is
328 inversely proportional to the size of the particle [18-21]. It creates a retardation force
329 that decreases the magnitude of the electrophoretic mobility of the particle if surface
330 conductivity is similar to or higher than the bulk electrical conductivity [18, 55].
331 Therefore, apparent zeta potentials (not corrected of surface conductivity) can be
332 significantly lower than true or intrinsic zeta potentials. Furthermore, Snoswell et al.
333 [22] made not a complete set of electrophoretic mobility measurements. These authors
334 therefore used an empirical interpolation formula to obtain zeta potentials at any pH and
335 ionic strength.



336

337 **Fig. 2.** Effect of the electrical double layer around the particle on the applied electrical
 338 field. Non-conducting particles (a.) and conducting particles (b.) (from Lyklema and
 339 Minor [55]). Du is the Dukhin number, which is defined as half the ratio of surface
 340 electrical conductivity to bulk electrical conductivity.

341

342 As shown by Eq. (5), the electrostatic potential at the OHP, ψ_d , is a key
 343 physicochemical parameter for describing the repulsive double layer interaction energy
 344 between TiO_2 NPs. In the double layer theory, the electrostatic potential at the OHP is
 345 usually assumed to be equal to the zeta potential (ζ) which can be inferred from
 346 electrophoretic mobility measurements, for example [19, 44]. Under the applied
 347 electrical field, hydrated counter-ions in the diffuse layer drag water molecules and
 348 therefore create a solvent flow at the surface of the particles. This solvent flow is
 349 therefore assumed to be zero at the onset of the diffuse layer which coincides with the
 350 shear plane where the zeta potential is located [19, 44].

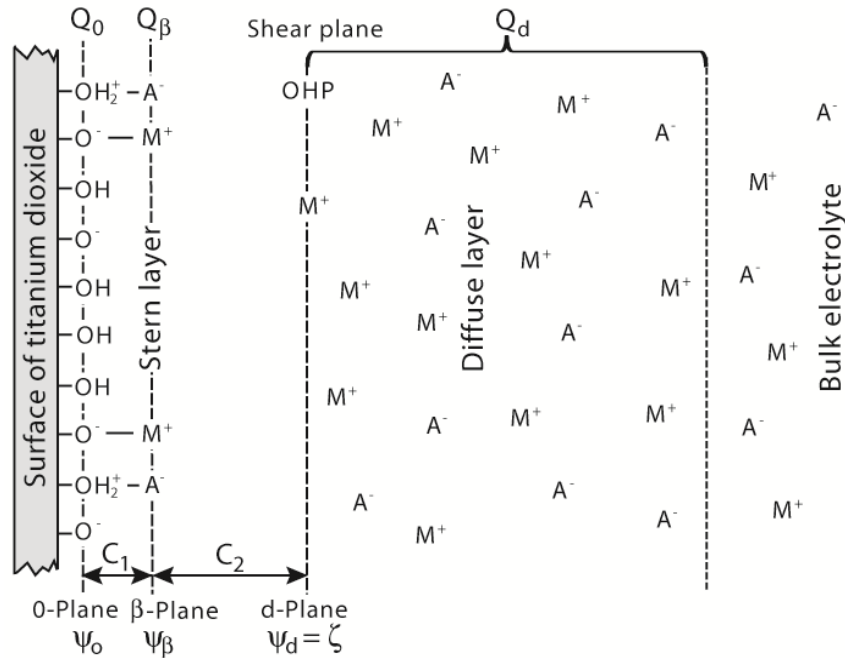
351 As opposed to what was done in previous studies [10, 22], the electrostatic potential at
 352 the OHP, ψ_d , is calculated directly by the extended Stern model of Leroy et al. [18]

1
2
3
4
5
6
7
8
9
10
11
12
13
14
15
16
17
18
19
20
21
22
23
24
25
26
27
28
29
30
31
32
33
34
35
36
37
38
39
40
41
42
43
44
45
46
47
48
49
50
51
52
53
54
55
56
57
58
59
60
61
62
63
64
65

353 (Fig. 3) and is therefore not derived directly from the electrophoretic mobility
354 measurements. The parameters of this electrostatic surface complexation model were
355 calibrated using ab-initio calculations (done with the Density Functional Theory, DFT),
356 crystallographic studies, electrophoretic mobility and potentiometric titration
357 measurements of pure TiO₂ NPs (Degussa P25) [8, 18]. Ridley et al. [25] emphasized
358 that the size and shape of TiO₂ nanoparticles have little influence on their measured
359 surface charge densities. In our approach, the electrochemical properties of the TiO₂
360 nanoparticles used by Snoswell et al. [22] are therefore assumed to be very close to the
361 electrochemical properties of the TiO₂ nanoparticles used by Leroy et al. [18]. This
362 justifies the use of the extended Stern model of Leroy et al. [18].

363 To confirm this assumption, we also use the approach of Leroy et al. [18] to convert
364 electrophoretic mobilities of Snoswell et al. [22] into zeta potentials using Henry's
365 electrokinetic transport model [56]. Therefore, experimental zeta potentials can be
366 compared to zeta potentials predicted by our electrostatic surface complexation model.

367 Because the two materials have slightly different pH_{IEP} (IEP is the isoelectric point, a
368 pH_{IEP} equal to 6.3 was reported in the work of Leroy et al. [18] and a pH_{IEP} equal to 6.1
369 was reported in the work of Snoswell et al. [22]), the value of the equilibrium constant
370 (K) for the sorption of protons at the $>Ti_2O^{-0.57}$ surface sites is modified (the initial value
371 of $\log K = 7.55$ [18] is replaced by $\log K = 7.1$).



372

373 **Fig. 3.** The simplified sketch of the extended Stern model (ESM) of Leroy et al. [18].

374 M^+ are metal cations (e.g., Na^+ or K^+) and A^- are anions (e.g., Cl^-). OHP is the outer

375 Helmholtz plane, which corresponds here to the shear plane where the zeta potential (ζ)

376 is defined. Q is the surface charge density of the three different layers (mineral surface,

377 Q_0 , Stern, Q_β , and diffuse layer, Q_d). C is the capacitance between the “0-plane” and

378 the “ β -plane” (C_1), and between the “ β -plane” and the “ d -plane” (C_2).

379

380 According to Henry [56], the surface conductivity and the internal conductivity of an

381 electrically charged particle alter the shape of the potential distribution of the applied

382 field in the liquid, modify the fluid motion within the electrical double layer, and

383 therefore change the fluid stresses exerted on the particle. For spherical particles, Henry

384 ([56]) proposed:

$$\zeta = \frac{3\eta}{2\varepsilon_0\varepsilon_r} \frac{1}{\{1 + 2\lambda[f(\kappa a) - 1]\}} \mu, \quad (10)$$

$$\lambda = \frac{1 - K' - 2Du}{2 + K' + 2Du}, \quad (11)$$

$$K' = \frac{\sigma_p}{\sigma_b}, \quad (12)$$

$$Du = \frac{\sigma_s}{2\sigma_b} = \frac{\Sigma_s}{a\sigma_b}, \quad (13)$$

385 where η is the dynamic viscosity of water (in Pa s; $\eta = 0.895 \times 10^{-3}$ Pa s at $T = 298$ K), λ
 386 is the dipolar coefficient of the particle, and $f(\kappa a)$ is a correction factor taking into
 387 account the retardation effect due to the size of the particle ([57], comprised between 1,
 388 Hückel theory [58], and 1.5, Smoluchowski theory [59]). σ is the electrical conductivity
 389 (in S m⁻¹), Σ is the specific surface electrical conductivity of the electrical double layer
 390 (in S), subscripts “*p*”, “*s*”, “*b*” correspond, respectively, to the particle’s “interior”
 391 (aggregates of elementary NPs), the particle’s surface and the surrounding medium (the
 392 bulk aqueous electrolyte). The specific surface conductivity expresses the excess of
 393 electrical conductivity at the solid’s surface compared to that of the bulk aqueous
 394 electrolyte [60-63]. Du corresponds to the Dukhin number (see Dukhin and Shilov [64]
 395 for more details concerning this parameter). Equations used for the calculation of the
 396 parameters $f(\kappa a)$, σ_p , σ_b , and Σ_s are written in Appendix B.

397 Electrophoretic mobilities are converted into true zeta potentials using Eqs. (10)-(13)
 398 and (B1)-(B8), in order to compare them with the ψ_d values calculated by our ESM.
 399 The fitting parameters for the conversion procedure are the radius of the aggregate
 400 (which varies with pH and salinity), a , the radius of elementary nanoparticles (which
 401 does not vary with pH and salinity), a_e and the intra-aggregate porosity ϕ , (the surface
 402 mobility of adsorbed counter-ions at the Stern layer is considered to be equal to their

403 mobility in bulk electrolyte). Specific surface conductivities of the Stern and diffuse
404 layers are estimated directly by our electrostatic surface complexation model.

405

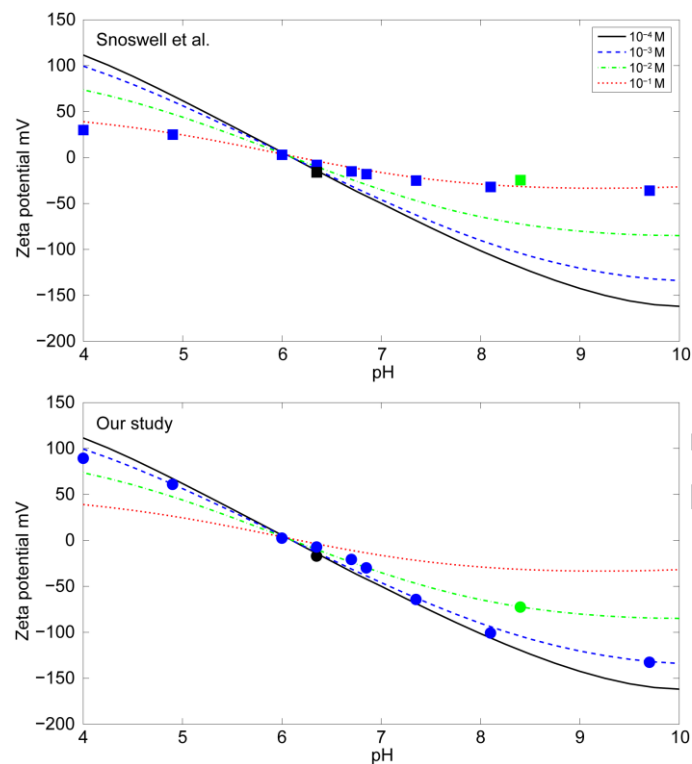
406 **3. Comparison with experimental data**

407 We test our approach combining an electrostatic surface complexation and an
408 aggregation kinetics model, to see if it could predict measured stability ratios of pure
409 synthetic TiO₂ NPs (immersed in a KCl solution at different pH values (6.3, 6.7 and 8.4)
410 [22]). The parameters required are the minimum separation distance between NPs, d_{\min} ,
411 the (non retarded) Hamaker constant, A_H , and the effective interaction radius, a_i . The
412 electrostatic potential ψ_d , which is directly calculated by the ESM, is compared to the
413 zeta potential inferred from the electrophoretic mobility measurements of Snoswell et
414 al. [22] using the approach of Leroy et al. [18]. Stability ratios predicted by LSA-DA,
415 and LSA-SEI are compared to the measured stability ratios of Snoswell et al. [22].

416

417 *3.1. Zeta potential*

418 The TiO₂ NPs zeta potentials reported by Snoswell et al. [22] and calculated with the
419 approach of Leroy et al. [18] are shown in Figs. 4a and 4b, respectively. Snoswell et al.
420 [22] used Henry's equation without surface conductivity correction (Eq. (10) with $\lambda =$
421 0.5) to estimate the zeta potentials from the measured electrophoretic mobilities. These
422 "observed" zeta potentials can be compared to the zeta potentials directly predicted by
423 the ESM (assuming $\psi_d = \zeta$). ESM calculations are done with PHREEQC [65].



ACCEPTED MANUSCRIPT

424

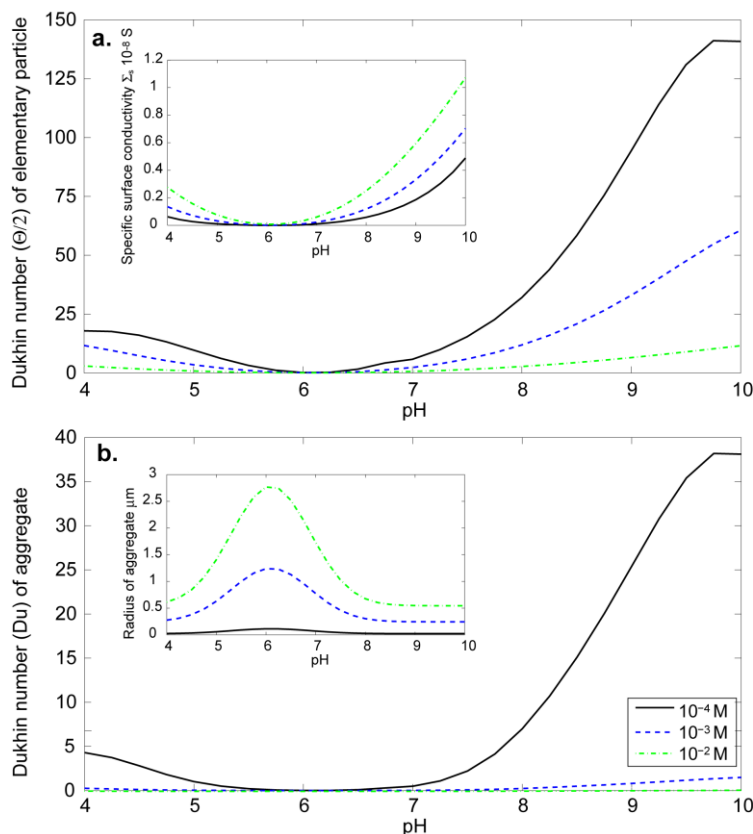
425 **Fig. 4.** “Observed” zeta potentials of pure TiO₂ NPs versus pH at 10^{-4} , 10^{-3} , and 10^{-2} M
 426 KCl from Snoswell et al. [22] (a; squares) and calculated using the approach of Leroy et
 427 al. [18] (b; circles). The curves are the ESM predictions assuming $\psi_d = \zeta$ [18].

428

429 Because of the strong influence of surface conductivity on the electrophoretic mobilities
 430 of TiO₂ NPs, zeta potentials estimated by Snoswell et al. [22] are significantly
 431 underestimated compared to the zeta potentials predicted by the surface complexation
 432 model (ESM), especially at low ionic strengths and pH values distant from the pH_{IEP}
 433 (pH_{IEP} = 6.1) (Fig. 4a). pH_{IEP} is the pH of isoelectric point. It is the pH value where the
 434 zeta potential is equal to zero.

435 This is not the case if the approach of Leroy et al. [18] is used to convert electrophoretic
 436 mobilities into zeta potentials taking into account surface conductivity (Fig. 4b).
 437 Underestimation of the true zeta potentials by Snoswell et al. [22] can be explained by
 438 the very high Dukhin number of the elementary NPs and their aggregated forms. This

439 high value of the surface conductivity of NPs compared to that of colloids and larger
 440 particles is readily justified because this phenomenon is inversely proportional to
 441 particle size [55] (Eqs. (13) and (B4)) (Fig. 5).



442
 443 **Fig. 5.** The predicted Dukhin numbers of (a) an elementary NP and (b) an aggregate
 444 versus pH at 10^{-4} , 10^{-3} , and 10^{-2} M KCl. The mean radius of elementary NPs is equal to
 445 6 nm ([22]), and the radius of the aggregate is optimized by decreasing the cost function
 446 $R^2 = \sum_{i=1}^L [\zeta_{\text{obs}}(i) - \psi_d(i)]^2$ using the Simplex algorithm [66] (where L is the number of
 447 experimental values). The intra-aggregate porosity is equal to 10 %.

448
 449 The Dukhin number increases as the ionic strength of the aqueous solution decreases
 450 because the ratio of surface to bulk electrical conductivity increases with the dilution of
 451 the aqueous electrolyte (Eq. (13)). Furthermore, when pH moves away from pH_{IEP} , the

452 Dukhin number increases because the specific surface conductivity increases (Fig. 4a).
453 This can be explained by the increasing concentration of counter-ions in the Stern and
454 diffuse layers (Eq. (B7); Γ_i^{St} and ψ_d increase when pH moves away from pH_{IEP}).
455 Snoswell et al. [22] significantly underestimated the true zeta potentials and therefore
456 the repulsive double layer energy between particles. This implies that, in their
457 aggregation kinetics modeling, they adjusted the Hamaker constant A_{H} with an
458 unrealistic value ($A_{\text{H}} = 2 \times 10^{-20}$ J for the $\text{TiO}_2\text{-H}_2\text{O-TiO}_2$ interface, see also section 1).
459 Their Hamaker constant is significantly lower than typical estimates. For instance,
460 Larson et al. [23] found $A_{\text{H}} = 6 \pm 2 \times 10^{-20}$ J for the $\text{TiO}_2\text{-H}_2\text{O-TiO}_2$ interface using the
461 DLVO theory and successfully predicted the interaction force between a rutile TiO_2
462 colloid (diameter of approximately 9 μm) and a single macroscopic rutile crystal in an
463 aqueous solution. This force was measured at the isoelectric point of the TiO_2 /water
464 interface (where no double layer interaction should occur) by Atomic Force Microscopy
465 (AFM). To date and to our knowledge, no study has shown that there is a correlation
466 between the Hamaker constant and particle size for metal oxide NPs. The calculations
467 done by Larson et al. [23] seriously question the value of the Hamaker constant deduced
468 by Snoswell et al. [22]. The A_{H} value found by Snoswell et al. [22] is also significantly
469 lower than the Hamaker constant estimated using spectroscopy data ($A_{\text{H}} = 7 \pm 1 \times 10^{-20}$ J
470 [23]) and the full Lifshitz theory ($A_{\text{H}} = 7.7 \pm 1.7 \times 10^{-20}$ J [24]; $A_{\text{H}} = 5.5 \pm 0.5 \times 10^{-20}$ J
471 [67]).

472

473 3.2. Aggregation kinetics

474 The evolution of the hydrodynamic radius of the aggregate with time (for a given
475 chemical composition of the aqueous solution) can be expressed by the stability ratio W .

476 This was determined experimentally by Snoswell et al. [22], who measured the ratio of
 477 the fast kinetic constant, k_f , to the slow kinetic constant, k_s . The two kinetic constants
 478 are proportional to the slope of the hydrodynamic radius a_h versus time t as $t \rightarrow 0$ s for
 479 each electrolyte concentration. Measured stability ratios enable the estimation of the
 480 critical coagulation concentration (CCC) [16]. The critical coagulation concentration is
 481 one of the most significant properties of NPs in suspension. It is defined as the
 482 minimum electrolyte concentration needed to induce fast aggregation of NPs, i.e. at
 483 CCC, the stability ratio is 1 ($\log(W)=0$).

484

485 3.2.1. *A priori parameters*

486 Our aggregation kinetics model involves four parameters: electrostatic potential at the
 487 OHP, ψ_d , minimum separation distance between NPs, d_{\min} , (non-retarded) Hamaker
 488 constant, A_H , and the particle's effective interaction radius, a_i . The electrostatic
 489 potential ψ_d is calculated by the ESM, whereas d_{\min} , A_H and a_i need to be optimized.
 490 As suggested by Frens and Overbeek [33], the minimum separation distance between
 491 NPs must be superior to twice the distance δ between the center of the surface atoms of
 492 the particle and the outer Helmholtz plane, i.e. $d_{\min} > 2\delta$. For $d \leq 2\delta$, counter-ions
 493 would be squeezed between the particles' surfaces. Such a violation of the
 494 electroneutrality of the double layer systems would give rise to a strong repulsion,
 495 which could not be overcome by the relatively weak van der Waals attraction between
 496 the particles. δ can be estimated using the following equation [68]:

$$\delta = \frac{\epsilon_0 \epsilon_{r1}}{C_1} + \frac{\epsilon_0 \epsilon_{r2}}{C_2}, \quad (14)$$

497 where C_1 and C_2 are capacitances (in F m^{-2}) of the two molecular capacitors of the ESM
 498 (Fig. 3). The first molecular capacitor corresponds to the interfacial region located
 499 between the “0-plane” and the “ β -plane” with a relative dielectric permittivity ε_{r1} (in F
 500 m^{-1}) while the second molecular capacitor corresponds to the region located between the
 501 “ β -plane” and the “ d -plane” with a relative dielectric permittivity ε_{r2} . In accordance
 502 with Bourikas et al. [9], and Hiemstra and Van Riemsdijk [68], we choose $\varepsilon_{r1} = 39.15$
 503 and $\varepsilon_{r2} = 78.3$. The value of ε_{r1} is half the value of ε_{r2} because of the presence of a
 504 strong electrical field between the “0-plane” and the “ β -plane”. The capacitance values
 505 are $C_1 = 2.5 \text{ F m}^{-2}$ and $C_2 = 1 \text{ F m}^{-2}$ [18]. Using Eq. (14) and the C and ε_r values given
 506 above, we obtain $\delta = 0.83 \text{ nm}$. This means that $d_{\min} > 1.66 \text{ nm}$.

507 The optimized values of the three parameters are determined using a MatLab routine
 508 and the Simplex algorithm [66] for which starting values are $d_{\min} = 1.66 \text{ nm}$,
 509 $A_{\text{H}} = 6 \times 10^{-20} \text{ J}$ [23] and $a_i = 150 \text{ nm}$. The a priori value of a_i is given according to
 510 dynamic light scattering measurements of TiO_2 primary particles in dilute water and for
 511 a pH value (not given by the authors) close to pH_{IEP} ($\text{pH}_{\text{IEP}} = 6.1$) [22].

512

513 3.2.2. Stability ratios

514 The Hamaker approach [45] and LSA [47] are used to calculate the interaction energies
 515 per unit area between two infinite flat plates due to van der Waals and double layer
 516 interactions (Eqs. (3) and (4), respectively). Interaction energies between two spherical
 517 particles with the same radius a_i were calculated accordingly using DA ([28]; Eqs.
 518 (A10) and (A11)) and SEI ([51]; Eqs. (A12)-(A16)). Stability ratios were determined

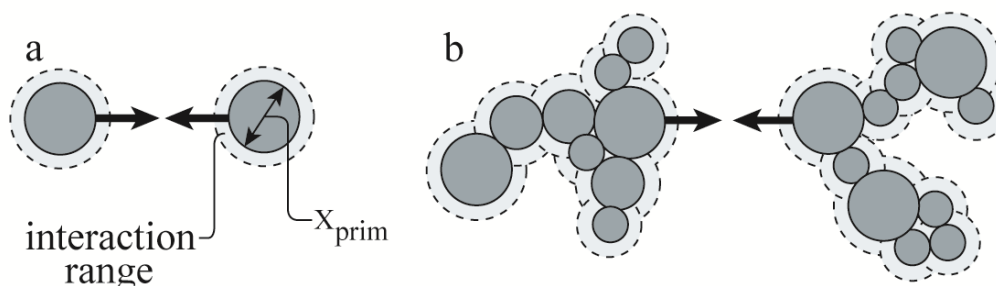
519 with Eqs. (1) and (2). The algorithm of optimization minimizes a cost function R^2
 520 defined in a least square sense:

$$R^2 = \sum_{i=1}^M \{\log[W_{\text{obs}}(i)] - \log[W_{\text{cal}}(i)]\}^2, \quad (15)$$

521 where M is the number of experimental values.

522 In the optimization procedure, two cases are considered. In the first case, the effective
 523 interaction radius is constant with pH. In the second case, the effective interaction
 524 radius varies with pH. As already stated by Snoswell et al. [22] and Schwarzer and
 525 Peukert [69], we suggest that the aggregation behavior of TiO₂ NPs can be controlled by
 526 NPs or small clusters of NPs with an effective interaction radius that can be shorter (low
 527 electrolyte concentration) or longer (high electrolyte concentration) than the Debye
 528 length. This implies that TiO₂ NPs aggregation kinetics can be controlled by
 529 nanoparticles or small clusters of nanoparticles rather than aggregates [22, 69].
 530 Schwarzer and Peukert [69] stated that, if the range of interaction (determined by at
 531 least two times the Debye length, κ^{-1}) is smaller than the size of the nanoparticle (this
 532 can be the case for an ionic strength greater than approximately 10^{-3} M where $\kappa^{-1} \cong 9.8$
 533 nm), the interaction energy of aggregates is determined only by the two nanoparticles
 534 involved (Fig. 6). Furthermore, Schwarzer and Peukert [69] emphasized that, if the
 535 range of interaction is similar to or longer than the size of the nanoparticle (this can be
 536 the case for an ionic strength lower than approximately 10^{-3} M because the Debye length
 537 increases with the dilution of the aqueous solution, see Eq. (6)), the interaction energy
 538 depends not only on the nanoparticles in contact but also on neighboring particles and
 539 their distance to contact, i.e. the local structure of the aggregate. This implies that the
 540 effective interaction radius can vary with ionic strength. Because stability ratios were
 541 recorded by Snoswell et al. [22] at different pH values with different salinity ranges, we

542 assume, like Snoswell et al. [22], that the effective interaction radius can vary with pH
 543 rather than with ionic strength (in order to limit the number of adjusted radii).

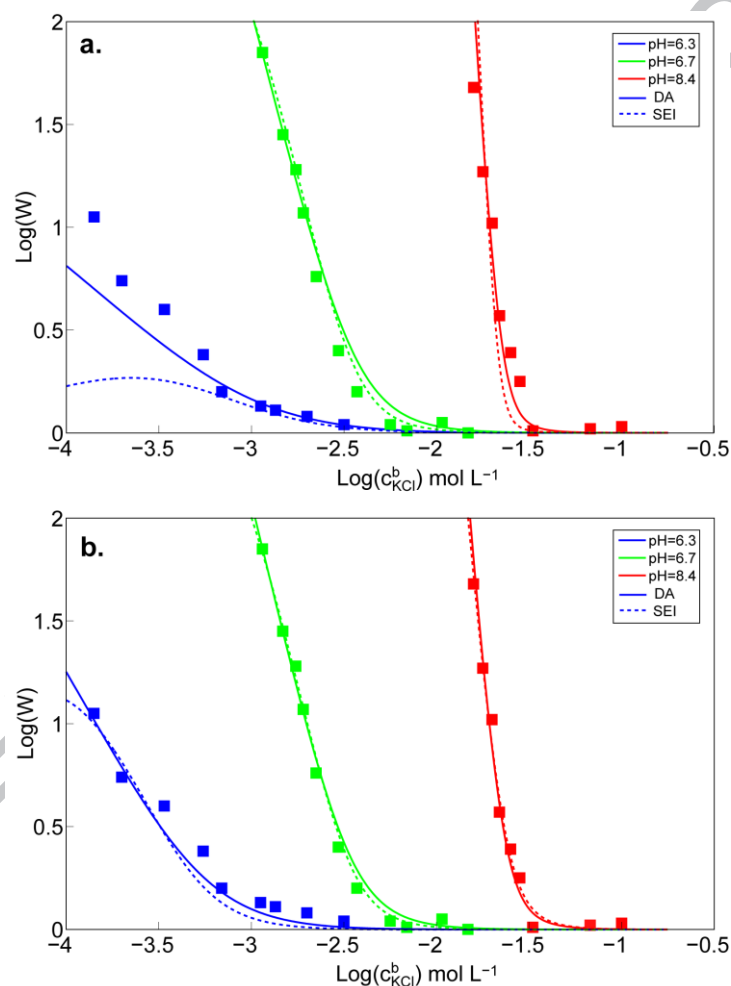


544
 545 **Fig. 6.** The aggregation behavior of two nanoparticles (a) and of two aggregates (b)
 546 showing that stability is determined by the two nanoparticles involved if the range of
 547 interaction (defined by the thickness of the diffuse layer) is largely inferior to their size
 548 (from Schwarzer and Peukert [69]).

549
 550 Stability ratios predicted using both approaches (DA and SEI) are in very good
 551 agreement with the experimental data of Snoswell et al. [22], except for the pH value
 552 very close to the pH_{IEP} ($\text{pH} = 6.3$) (Fig. 7). When the effective interaction radius is
 553 considered to vary with pH, our stability ratio predictions improve significantly,
 554 particularly at $\text{pH} = 6.3$ and for ionic strengths lower than approximately 10^{-3} M.
 555 According to Schwarzer and Peukert [69], at low ionic strengths, the local structure of
 556 the aggregate can control its aggregation behavior. Therefore, under these
 557 physicochemical conditions, a larger effective interaction radius is needed to reproduce
 558 the trend of the experimental data (according to the DLVO theory, predicted stability
 559 ratios increase with the radius of the particle [16]).

560 At $\text{pH} = 6.3$, a combination of LSA and DA gives better predictions of stability ratios
 561 than a combination of LSA and SEI. LSA is very good for large separation distances
 562 and less efficient for small separation distances while DA overestimates the interaction

563 energy for large separation distances but is efficient for small separation distances.
 564 Consequently, the LSA-DA combination is a good compromise that covers all of the
 565 separating distances between particles [47, 50]. The present approach can also
 566 accurately predict CCC, which increases with pH. This can be explained by the
 567 increasing magnitude of the surface electrical potential and repulsive double layer force
 568 when pH moves away from pH_{IEP} (Fig. 4).



569 **Fig. 7.** Stability ratios versus salinity (KCl) (in log scale) at three different pH values
 570 (pH = 6.3, 6.7, and 8.4). Experimental data from Snoswell et al. [22] (squares) and
 571 model predictions with DA (solid lines) and SEI (dotted lines). Two cases are
 572 considered: the effective interaction radius is constant with pH (a) and the effective
 573 interaction radius varies with pH (b).
 574

575

1
2 576 During slow aggregation, also called reaction limited clusters aggregation (RLCA) [16],
3
4
5 577 there is a strong electrostatic barrier between particles, $\log(W) > 0$, and the aggregation
6
7 578 rate depends strongly on the salt concentration (Fig. 7). In that case, not all collisions
8
9
10 579 lead to sticking events, and individual particles have time to find a pathway into the
11
12 580 core of a compact aggregate [16, 70] (mass fractal dimension $D = 2.1-2.2$ [70]). During
13
14 581 fast aggregation, also called diffusion limited clusters aggregation (DLCA), the
15
16 582 interaction energy between particles is purely attractive (due to van der Waals
17
18 583 interactions), $\log(W) = 0$, and the aggregation rate no longer depends on the salt
19
20 584 concentration (Fig. 7). In that case, diffusion of clusters controls the aggregation process
21
22 585 [16], leading to larger and less compact aggregates (compared to RLCA; mass fractal
23
24 586 dimension $D = 1.7-1.8$ [70]). In the intermediate phase between slow and fast
25
26 587 aggregation, there is a gradual transition between RLCA and DLCA [16, 70].

27
28
29
30 588 The quality of the stability ratio predictions decreases when the pH of the solution is
31
32 589 close to pH_{IEP} (at $\text{pH} = 6.3$) and when the salinity is close to the CCC. It is very difficult
33
34 590 to reproduce the evolution of stability ratios when the pH of the aqueous solution is
35
36 591 close to pH_{IEP} and in the transition phase between the slow and fast aggregation [10, 16,
37
38 592 70]. This is because, under these physicochemical conditions, repulsive double layer
39
40 593 forces are relatively weak compared to attractive van der Waals forces and, therefore,
41
42 594 TiO_2 NPs aggregation kinetics may be controlled by the collision of more than two
43
44 595 isolated particles [40, 71].
45
46
47
48
49
50

596

597 *3.2.3. Optimized parameters and interaction energy profiles*

1
2
3
4
5
6
7
8
9
10
11
12
13
14
15
16
17
18
19
20
21
22
23
24
25
26
27
28
29
30
31
32
33
34
35
36
37
38
39
40
41
42
43
44
45
46
47
48
49
50
51
52
53
54
55
56
57
58
59
60
61
62
63
64
65

598 Values of adjusted parameters are given in Table 1 (constant effective interaction
599 radius) and Table 2 (variable effective interaction radius). In all cases, the minimum
600 separation distance is significantly greater than the a priori value (1.66 nm). This might
601 be due to the uncertainty associated with the estimation of δ . Indeed, in Eq. (14), the
602 dielectric permittivities ϵ_{r1} , ϵ_{r2} , and the capacitance C_2 are not precisely known [68].
603 The capacitance C_2 remains relatively unknown because the dielectric permittivity ϵ_{r2}
604 and the location of the shear plane (where the zeta potential is located) are still uncertain
605 [55] ($C_2 = \epsilon_{r2}/(x_d - x_\beta)$ where x_β and x_d are the locations of the “ β -plane” and the “ d -
606 plane”, which corresponds to the shear plane, from the TiO_2 's surface). A second reason
607 for the large d_{\min} value might be an overestimation of the electrostatic potential ψ_d by
608 our ESM. The capacitance C_2 of our ESM is the parameter most subject to some
609 uncertainty because, as cited above, the location of the shear plane remains relatively
610 unknown. A lower capacitance C_2 value would lead to a lower magnitude of the
611 electrostatic potential ψ_d . A third reason might be due to the DLVO theory, which
612 overestimates interaction energies between NPs [22, 29, 37], in particular for small
613 separation distances. Indeed, it has been observed that the DLVO theory overestimates
614 interaction energies between TiO_2 particles for small separation distances [23]. For
615 example, Larson et al. [23] found a good agreement between surface force
616 measurements and predictions (with the DLVO theory) at a minimum separation
617 distance of only 10 nm.

618 When the effective interaction radius is assumed to vary with pH, d_{\min} decreases
619 compared to the case when the effective interaction radius is assumed to be constant
620 with pH (Table 2). Furthermore, when a_i varies with pH, our stability ratio predictions

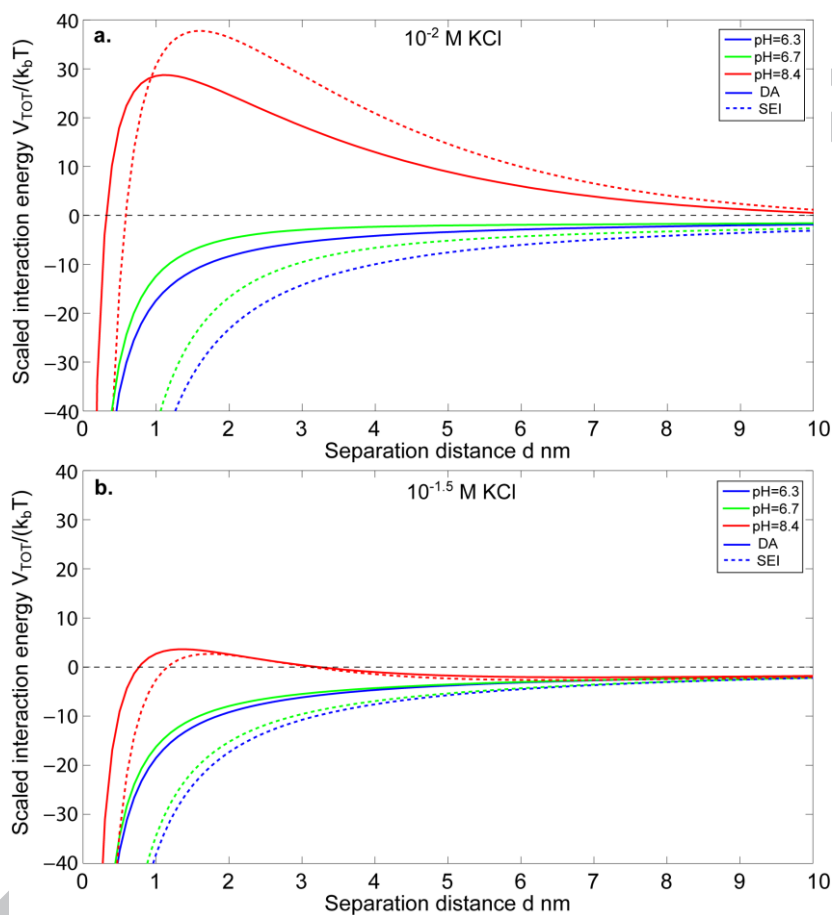
621 are almost entirely independent of the value of d_{\min} chosen (Table 2; the cost function
622 R^2 increases slightly as the d_{\min} value decreases). This implies that considering an
623 effective interaction radius that varies with pH not only increases the accuracy of our
624 stability ratio predictions, but it also decreases significantly the dependence of our
625 stability ratio predictions on the value of d_{\min} .

626 The optimized Hamaker constant and radius given by SEI are greater than those given
627 by DA. This is because DA overestimates the van der Waals and double layer
628 interaction energies of small particles (relative to the Debye length) compared to SEI
629 [51]. Aside from this disagreement between DA and SEI in the estimation of the
630 parameters, on the contrary to Snoswell et al. [22], the optimized Hamaker constants are
631 similar to values found in the literature [23, 24, 67].

632 When the effective interaction radius is assumed to be constant with pH (Fig. 7a), its
633 optimized values are close to the mean radius of the surface crystallites that constitute
634 the aggregate (a_e is between 6 and 20 nm according to Snoswell et al. [22]; Table 1).
635 This implies that TiO₂ NPs aggregation kinetics are controlled by surface crystallites or
636 small clusters of surface crystallites rather than by aggregates, as reported by Schwarzer
637 and Peukert [69]. When the effective interaction radius is assumed to vary with pH (Fig.
638 7b), its optimized values increase with the dilution of the aqueous solution (Table 2).
639 These results agree with the statements of Schwarzer and Peukert [69] who emphasized
640 that, if the range of interaction is similar to or longer than the size of the nanoparticle,
641 the interaction energy will depend on the local structure of the aggregate.

642 Interaction energy profiles calculated using the two approaches (DA and SEI) for the
643 three pH values and for a salinity of 10^{-2} M KCl, are shown in Fig. 8a. This salinity
644 corresponds approximately to CCC at pH = 6.7 (Fig. 7). For low pH values (pH = 6.3,

645 6.7), the interaction energies between particles are only attractive because repulsive
 646 double layer forces are weak compared to van der Waals forces. At a higher ionic
 647 strength, $10^{-1.5}$ M KCl (which corresponds approximately to CCC at pH = 8.4), the
 648 repulsive energy barrier at pH = 8.4 disappears almost entirely (Fig. 8b).



649
 650 **Fig. 8.** Interaction energy profiles calculated by DA (solid lines) and SEI (dotted lines)
 651 at three different pH values (pH = 6.3, 6.7, and 8.4) and in the case of a constant
 652 effective interaction radius. **a.** Salinity of 10^{-2} M KCl. **b.** Salinity of $10^{-1.5}$ M KCl.

653
 654 Our results show that the DA method is easily adjustable with three parameters
 655 (minimum separation distance, Hamaker constant, and effective interaction radius)
 656 while the SEI method is theoretically more suitable for NPs due to their nanometric size
 657 [51]. Moreover, considering an effective interaction radius that decreases with pH

1
2
3
4
5
6
7
8
9
10
11
12
13
14
15
16
17
18
19
20
21
22
23
24
25
26
27
28
29
30
31
32
33
34
35
36
37
38
39
40
41
42
43
44
45
46
47
48
49
50
51
52
53
54
55
56
57
58
59
60
61
62
63
64
65

658 increases significantly the accuracy of our stability ratio predictions. Our results do not
659 agree with the effective interaction radii obtained by Snoswell et al. [22], whose
660 optimized effective interaction radius increases with the pH of the aqueous solution
661 (they found a_i values of 6, 12, and 20 nm at pH levels of 6.3, 6.7, and 8.4,
662 respectively). In our approach, the introduction of true zeta potentials predicted by our
663 extended Stern model reversed this trend because the retardation effect of surface
664 conductivity is more pronounced when the ionic strength of the aqueous solution is low
665 and the pH is distant from pH_{IEP} . We also find realistic values of Hamaker constants for
666 the $\text{TiO}_2\text{-H}_2\text{O-TiO}_2$ interface. The approach proposed here appears, therefore, to be a
667 real improvement, reaching a quantitative agreement with experimental results while
668 using realistic parameterization.

669

670 4. Conclusions

671 We have developed a new approach based on DLVO theory to describe aggregation
672 kinetics of titanium dioxide nanoparticles (NPs) in aqueous solutions. It has the
673 advantage of using zeta potentials directly calculated by an extended Stern model
674 (ESM) because metal oxide NPs have a very high surface electrical conductivity which
675 slows down their electrophoretic motion. Linear superposition approximation (LSA) is
676 combined with Derjaguin approximation (DA) or surface element integration (SEI) to
677 calculate interaction energies of spherical particles.

678 Zeta potentials calculated by our ESM and inferred from electrophoretic mobilities
679 taking into account surface conductivity are found to be significantly higher in
680 amplitude than apparent zeta potentials (not corrected for surface conductivity). Our
681 work shows that the repulsive electrostatic force between NPs and their stability ratios

682 can be significantly underestimated if apparent zeta potentials are used instead of true
683 zeta potentials.

684 Our two aggregation kinetics models (DA and SEI) are validated against measured
685 stability ratios of pure synthetic TiO₂ NPs made at different pH values (pH = 6.3, 6.7,
686 and 8.4) over a broad salinity range (between 10⁻⁴ and 10⁻¹ M KCl). Optimized
687 Hamaker constants, comprised between 5.89 and 8.71×10⁻²⁰ J, are in agreement with
688 those reported in the literature. This confirms that DLVO theory is relevant to predict
689 aggregation kinetics of TiO₂ NPs if the zeta potential is estimated accurately. Our model
690 can also be used to predict stability ratios of TiO₂ NPs at other pH values because it
691 doesn't need electrophoretic mobility measurements.

692 The DA and SEI methods predict similar stability ratios, except at the lowest ionic
693 strengths (lower to 10⁻³ M KCl) because DA overestimates significantly interaction
694 energies when the interaction range can be similar to or longer than the size of
695 nanoparticles. We also find that, in these physicochemical conditions, TiO₂ NPs
696 aggregation kinetics are controlled by the local structure of the aggregate, whereas, at
697 high ionic strengths, when the interaction range is shorter than the size of the
698 nanoparticles, TiO₂ NPs aggregation kinetics are controlled by nanoparticles.

699 In the future, our approach can be used to predict the stability ratios of TiO₂ NPs
700 immersed in other aqueous electrolytes and to predict the stability ratios of other metal
701 oxides NPs. It can also be used to better understand the contribution of each process
702 (aggregation, deposition) that affects the mobility of NPs in a flow-through column
703 experiment. It can also contribute to quantitatively estimating the effect of the chemical
704 composition of pore water (pH, ionic strength, the chemical nature of dissolved species)
705 on the NPs reactive transport processes in porous media.

706

707 **Acknowledgments**

1
2 708 This paper is a part of the PhD thesis of Izzeddine Sameut Bouhaik, which is co-funded
3
4
5 709 by the Carnot Institute –BRGM and the Region Centre. We would like to thank the
6
7 710 editor and the anonymous reviewers for their efforts and constructive comments that
8
9 711 contributed to improving our manuscript.
10
11
12 712

ACCEPTED MANUSCRIPT

713 **Appendix A**

714 According to Derjaguin approximation, interaction energy V between two spherical
 715 particles can be expressed as a function of the interaction energy per unit area between
 716 two infinite flat plates E by:

$$V_{\text{DA}}(d) \approx \int_d^{\infty} 2\pi r E(h) dr, \quad (\text{A1})$$

717 where d is the separation distance between the two spherical particles of radii a_1 and a_2
 718 (see Fig. 1). The distance between two elements of surface, h , can be written by:

$$h = H \pm z_1 \pm z_2, \quad (\text{A2})$$

719 where H is the distance between the centers of the two spherical particles of coordinates
 720 z_1 and z_2 . Eq. (A2) can be written again by:

$$h = H \pm a_1 \left(\sqrt{1 - r^2/a_1^2} \right) \pm a_2 \left(\sqrt{1 - r^2/a_2^2} \right). \quad (\text{A3})$$

721 Eq. (A3) can be simplified if the two closest surfaces (PAQ-PAQ) are only taken into
 722 account. This leads to:

$$h = H - a_1 \left(\sqrt{1 - r^2/a_1^2} \right) - a_2 \left(\sqrt{1 - r^2/a_2^2} \right). \quad (\text{A4})$$

723 Derivative of Eq. (A4) gives:

$$dh = \left\{ \frac{1}{a_1 \left[\sqrt{1 - r^2/a_1^2} \right]} + \frac{1}{a_2 \left[\sqrt{1 - r^2/a_2^2} \right]} \right\} r dr. \quad (\text{A5})$$

724 In the DA approach, radii are significantly larger than interaction distance. This implies:

$$\min(a_1, a_2) \gg r. \quad (\text{A6})$$

725 Therefore, by considering approximation (A6) in Eq. (A5), it follows:

$$dh \approx \left(\frac{1}{a_1} + \frac{1}{a_2} \right) r dr, \quad (\text{A7})$$

$$r dr \approx \left(\frac{a_1 a_2}{a_1 + a_2} \right) dh. \quad (\text{A8})$$

726 Finally, by combining Eqs. (A1) and (A8), the final DA equation is obtained:

$$V_{\text{DA}}(d) \approx \frac{2\pi a_1 a_2}{a_1 + a_2} \int_d^{\infty} E(h) dh. \quad (\text{A9})$$

727 By combining Eqs. (3) and (A9), the attractive van der Waals interaction energy
728 between two spherical particles can be calculated by [28]:

$$V_{\text{VDW}}^{\text{DA}} = -\frac{A_{\text{H}} a_1 a_2}{6d(a_1 + a_2)}. \quad (\text{A10})$$

729 The repulsive interaction energy due to the overlapping of the diffuse layers of the two
730 spherical particles is estimated by combining Eqs. (4) and (A9):

$$V_{\text{EDL}}^{\text{DA}} = 64\pi\epsilon_0\epsilon_r y_1 y_2 \frac{a_1 a_2}{a_1 + a_2} \left(\frac{kT}{ze} \right)^2 e^{-\kappa d}. \quad (\text{A11})$$

731 In the case of the surface element integration method, we can separate the surface of
732 each particle (S_1 and S_2) into two hemispherical surfaces (PAQ and PA'Q) (Fig. 1).
733 Four interaction energy terms are needed to calculate the total interaction energy
734 between the two surfaces (S_1 and S_2). The signs of these terms depend on the different
735 combinations of the signs of $\mathbf{n}_1 \cdot \mathbf{k}_1$ and $\mathbf{n}_2 \cdot \mathbf{k}_2$. The total interaction energy is the sum
736 of all four interaction energy terms. The total interaction energy between two spherical
737 particles, V_{SEI} , can be calculated by [51]:

$$V_{\text{SEI}} = V_1 - V_2 - V_3 + V_4, \quad (\text{A12})$$

738 where V_i ($i=1, 2, 3, 4$) is the surface-surface interaction energy. It can be written as:

$$V_1 = 2\pi \int_0^{a_1} \left(\sqrt{1 - r^2/a_2^2} \right) E \left(d + a_1 + a_2 - a_1 \sqrt{1 - r^2/a_1^2} - a_2 \sqrt{1 - r^2/a_2^2} \right) r \, dr, \quad (\text{A13})$$

$$V_2 = 2\pi \int_0^{a_1} \left(\sqrt{1 - r^2/a_2^2} \right) E \left(d + a_1 + a_2 + a_1 \sqrt{1 - r^2/a_1^2} - a_2 \sqrt{1 - r^2/a_2^2} \right) r \, dr, \quad (\text{A14})$$

$$V_3 = 2\pi \int_0^{a_1} \left(\sqrt{1 - r^2/a_2^2} \right) E \left(d + a_1 + a_2 - a_1 \sqrt{1 - r^2/a_1^2} + a_2 \sqrt{1 - r^2/a_2^2} \right) r \, dr, \quad (\text{A15})$$

$$V_4 = 2\pi \int_0^{a_1} \left(\sqrt{1 - r^2/a_2^2} \right) E \left(d + a_1 + a_2 + a_1 \sqrt{1 - r^2/a_1^2} + a_2 \sqrt{1 - r^2/a_2^2} \right) r \, dr, \quad (\text{A16})$$

739 where E is the interaction energy per unit area between two infinite flat plates separated
 740 by a distance h and is expressed by Eqs. (3) and (4) for VDW and EDL interactions,
 741 respectively.

742

743 **Appendix B**

744 Ohshima [57] developed a very useful analytical equation to accurately estimate $f(\kappa a)$
 745 as a function of the particle size and Debye length:

$$f(\kappa a) = 1 + \frac{1}{2(1 + \delta/\kappa a)^3}, \quad (\text{B1})$$

746 where δ can be described by:

$$\delta = \frac{2.5}{1 + 2e^{-\kappa a}}. \quad (\text{B2})$$

747 The internal conductivity of the particle, σ_p , can be estimated using the so-called
 748 differential self-consistent model applied for disk-shaped particles [61, 63]:

$$\sigma_p = \frac{\sigma_b}{F} \left[F\Theta + \frac{1}{2}(1-\Theta) \left(1 - \Theta + \sqrt{(1-\Theta)^2 + 4F\Theta} \right) \right], \quad (\text{B3})$$

$$\Theta = \frac{\sigma_e}{\sigma_b} = \frac{2\Sigma_s}{a_e\sigma_b}, \quad (\text{B4})$$

$$F = \phi^{-2}, \quad (\text{B5})$$

749 where a_e is the radius of elementary NP and ϕ is the intra-aggregate porosity. Eq. (B3)

750 has the advantage of not being restricted to any κa_e values.

751 The electrical conductivity of bulk water, σ_b , is calculated by:

$$\sigma_b = \sum_{i=1}^N e1000N_A z_i \beta_i^b c_i^b, \quad (\text{B6})$$

752 where N is the number of types of ions and β_i^b is the ionic mobility in bulk water (in m^2
 753 $\text{s}^{-1} \text{V}^{-1}$).

754 The specific surface conductivity, Σ_s , due to the electromigration of counter-ions in the

755 Stern layer and to the electromigration of hydrated counter-ions and co-ions in the

756 diffuse layer, can be calculated as a function of pH and salinity using Revil and
 757 Glover's electrokinetic transport model [60]:

$$\Sigma_s = \sum_i z_i e \beta_i^{\text{St}} \Gamma_i^{\text{St}} + 2\kappa^{-1} e 1000 N_A z \left\{ \left(c_{(+)}^b B_{(+)} + c_{\text{H}^+}^b B_{\text{H}^+} \right) \left[\exp\left(\frac{-ez\psi_d}{2k_b T}\right) - 1 \right] \right. \\ \left. + \left(c_{(-)}^b B_{(-)} + c_{\text{OH}^-}^b B_{\text{OH}^-} \right) \left[\exp\left(\frac{ez\psi_d}{2k_b T}\right) - 1 \right] \right\}, \quad (\text{B7})$$

$$B_i = \beta_i^b + \frac{2\varepsilon_0 \varepsilon_r k_b T}{\eta e z_i}, \quad (\text{B8})$$

758 where β_i^{St} is the ionic mobility of adsorbed counter-ions at the Stern layer (in $\text{m}^2 \text{s}^{-1} \text{V}^{-1}$), Γ_i^{St} is their surface site density (in sites m^{-2}), and “+” and “-” stand for cations and
 759 anions, respectively. As shown in Eq. (B7), the specific surface conductivity, Σ_s ,
 760 depends on the surface site density of adsorbed counter-ions at the Stern layer, Γ_i^{St} , and
 761 on the electrostatic potential at the OHP, ψ_d . Γ_i^{St} and ψ_d can be calculated using an
 762 extended Stern model (ESM, Fig. 3), which describes the electrochemical properties of
 763 the $\text{TiO}_2/\text{water}$ interface [8, 18].

764
 765

766 **Figure captions**

1
2 767 **Fig. 1.** Two interacting spherical particles with radii a_1 and a_2 . The centers of the
3
4 768 spheres are origins of two body-fixed coordinate systems, with their z axes directly
5
6 769 facing each other. The xy planes of these coordinate systems are parallel to each other
7
8 770 (from Bhattacharjee et al. [51]).

9
10
11 771 **Fig. 2.** Effect of the electrical double layer around the particle on the applied electrical
12
13 772 field. Non-conducting particles (**a.**) and conducting particles (**b.**) (from Lyklema and
14
15 773 Minor [55]). Du is the Dukhin number, which is defined as half the ratio of surface
16
17 774 electrical conductivity to bulk electrical conductivity.

18
19 775 **Fig. 3.** The simplified sketch of the extended Stern model (ESM) of Leroy et al. [18].
20
21 776 M^+ are metal cations (e.g., Na^+ or K^+) and A^- are anions (e.g., Cl^-). OHP is the outer
22
23 777 Helmholtz plane, which corresponds here to the shear plane where the zeta potential (ζ)
24
25 778 is defined. Q is the surface charge density of the three different layers (mineral surface,
26
27 779 Q_0 , Stern, Q_β , and diffuse layer, Q_d). C is the capacitance between the “0-plane” and
28
29 780 the “ β -plane” (C_1), and between the “ β -plane” and the “ d -plane” (C_2).

30
31 781 **Fig. 4.** “Observed” zeta potentials of pure TiO_2 NPs versus pH at 10^{-4} , 10^{-3} , and 10^{-2} M
32
33 782 KCl from Snoswell et al. [22] (**a**; squares) and calculated using the approach of Leroy et
34
35 783 al. [18] (**b**; circles). The curves are the ESM predictions assuming $\psi_d = \zeta$ [18].

36
37 784 **Fig. 5.** The predicted Dukhin numbers of (**a**) an elementary NP and (**b**) an aggregate
38
39 785 versus pH at 10^{-4} , 10^{-3} , and 10^{-2} M KCl. The mean radius of elementary NPs is equal to
40
41 786 6 nm ([22]), and the radius of the aggregate is optimized by decreasing the cost function

42
43 787 $R^2 = \sum_{i=1}^L [\zeta_{obs}(i) - \psi_d(i)]^2$ using the Simplex algorithm [66] (where L is the number of
44
45 788 experimental values). The intra-aggregate porosity is equal to 10 %.

1
2
3
4
5
6
7
8
9
10
11
12
13
14
15
16
17
18
19
20
21
22
23
24
25
26
27
28
29
30
31
32
33
34
35
36
37
38
39
40
41
42
43
44
45
46
47
48
49
50
51
52
53
54
55
56
57
58
59
60
61
62
63
64
65

789 **Fig. 6.** The aggregation behavior of two nanoparticles (**a**) and of two aggregates (**b**)
790 showing that stability is determined by the two nanoparticles involved if the range of
791 interaction (defined by the thickness of the diffuse layer) is largely inferior to their size
792 (from Schwarzer and Peukert [69]).

793 **Fig. 7.** Stability ratios versus salinity (KCl) (in log scale) at three different pH values
794 (pH = 6.3, 6.7, and 8.4). Experimental data from Snoswell et al. [22] (squares) and
795 model predictions with DA (solid lines) and SEI (dotted lines). Two cases are
796 considered: the effective interaction radius is constant with pH (**a**) and the effective
797 interaction radius varies with pH (**b**).

798 **Fig. 8.** Interaction energy profiles calculated by DA (solid lines) and SEI (dotted lines)
799 at three different pH values (pH = 6.3, 6.7, and 8.4) and in the case of a constant
800 effective interaction radius. **a.** Salinity of 10^{-2} M KCl. **b.** Salinity of $10^{-1.5}$ M KCl.

802 **References**

- 1
2 803 [1] M.R. Wiesner, G.V. Lowry, P. Alvarez, D. Dionysiou, P. Biswas, *Environ. Sci.*
3
4 804 *Technol.* 40 (2006) 4336.
5
6
7 805 [2] A.R. Petosa, D.P. Jaisi, I.R. Quevedo, M. Elimelech, N. Tufenkji, *Environ. Sci.*
8
9 806 *Technol.* 44 (2010) 6532.
10
11 807 [3] H.F. Lecoanet, J.Y. Bottero, M.R. Wiesner, *Environ. Sci. Technol.* 38 (2004)
12
13 808 5164.
14
15
16 809 [4] B. Nowack, T.D. Bucheli, *Environ. Pollut.* 150 (2007) 5.
17
18 810 [5] P. Biswas, C.Y. Wu, *J. Air Waste Manage.* 55 (2005) 708.
19
20
21 811 [6] H.F. Lecoanet, M.R. Wiesner, *Environ. Sci. Technol.* 38 (2004) 4377.
22
23 812 [7] K.A.D. Guzman, M.P. Finnegan, J.F. Banfield, *Environ. Sci. Technol.* 40 (2006)
24
25 813 7688.
26
27
28 814 [8] G.D. Panagiotou, T. Petsi, K. Bourikas, C.S. Garoufalis, A. Tsevis, N. Spanos, C.
29
30 815 Kordulis, A. Lycourghiotis, *Adv. Colloid Interface Sci.* 142 (2008) 20.
31
32 816 [9] K. Bourikas, T. Hiemstra, W. Van Riemsdijk, *Langmuir* (2001) 749.
33
34 817 [10] X.Y. Liu, G.X. Chen, C.M. Su, *J. Colloid Interface Sci.* 363 (2011) 84.
35
36 818 [11] R.A. French, A.R. Jacobson, B. Kim, S.L. Isley, R.L. Penn, P.C. Baveye, *Environ.*
37
38 819 *Sci. Technol.* 43 (2009) 1354.
39
40
41 820 [12] Y. Zhang, Y.S. Chen, P. Westerhoff, J. Crittenden, *Water. Res.* 43 (2009) 4249.
42
43 821 [13] J.M. Herrmann, *Catal. Today* 53 (1999) 115.
44
45 822 [14] M.R. Hoffmann, S.T. Martin, W.Y. Choi, D.W. Bahnemann, *Chem. Rev.* 95
46
47 823 (1995) 69.
48
49 824 [15] E.M. Hotze, T. Phenrat, G.V. Lowry, *J. Environ. Qual.* 39 (2010) 1909.
50
51 825 [16] M. Elimelech, J. Gregory, X. Jia, R.A. Williams, Butterworth-Heinemann,
52
53 826 Boston, 1995, 448p.
54
55
56
57
58
59
60
61
62
63
64
65

- 1
2
3
4
5
6
7
8
9
10
11
12
13
14
15
16
17
18
19
20
21
22
23
24
25
26
27
28
29
30
31
32
33
34
35
36
37
38
39
40
41
42
43
44
45
46
47
48
49
50
51
52
53
54
55
56
57
58
59
60
61
62
63
64
65
- 827 [17] N. Solovitch, J. Labille, J. Rose, P. Chaurand, D. Borschneck, M.R. Wiesner, J.Y.
828 Bottero, *Environ. Sci. Technol.* 44 (2010) 4897.
- 829 [18] P. Leroy, C. Tournassat, M. Bizi, *J. Colloid Interface Sci.* 356 (2011) 442.
- 830 [19] J. Lyklema, Academic Press, London, 1991, 736p.
- 831 [20] J.J. Bikerman, *Trans. Faraday Soc.* 35 (1940) 154.
- 832 [21] A. Crespy, A. Boleve, A. Revil, *J. Colloid Interface Sci.* (2007) 188.
- 833 [22] D.R.E. Snoswell, J.M. Duan, D. Fornasiero, J. Ralston, *Int. J. Miner. Process.* 78
834 (2005) 1.
- 835 [23] I. Larson, C.J. Drummond, D.Y.C. Chan, F. Grieser, *J. Am. Chem. Soc.* 115
836 (1993) 11885.
- 837 [24] H.D. Ackler, R.H. French, Y.M. Chiang, *J. Colloid Interface Sci.* 179 (1996) 460.
- 838 [25] M.K. Ridley, V.A. Hackley, M.L. Machesky, *Langmuir* 22 (2006) 10972.
- 839 [26] A.M. Puertas, F.J. de las Nieves, *J. Colloid Interface Sci.* 216 (1999) 221.
- 840 [27] E.J.W. Verwey, J.T.G. Overbeek, Elsevier, Amsterdam, 1948, 218p.
- 841 [28] B.V. Derjaguin, L. Landau, *Acta Physicochim. USSR.* 14 (1941) 633.
- 842 [29] H. Kihira, N. Ryde, E. Matijevic, *Colloid Surf.* 64 (1992) 317.
- 843 [30] N. Kallay, T. Preocanin, D. Kovacevic, *Croat. Chem. Acta* 82 (2009) 531.
- 844 [31] S.Y. Shulepov, *J. Colloid Interface Sci.* 189 (1997) 199.
- 845 [32] S.S. Dukhin, J. Lyklema, *Langmuir* 3 (1987) 94.
- 846 [33] G. Frens, J.T.G. Overbeek, *J. Colloid Interface Sci.* 38 (1972) 376.
- 847 [34] J. Israelachvili, H. Wennerstrom, *Nature* 379 (1996) 219.
- 848 [35] P. Kekicheff, O. Spalla, *Phys. Rev. Lett.* 75 (1995) 1851.
- 849 [36] S.Y. Shulepov, G. Frens, *J. Colloid Interface Sci.* 182 (1996) 388.
- 850 [37] S.H. Behrens, D.I. Christl, R. Emmerzael, P. Schurtenberger, M. Borkovec,
851 *Langmuir* 16 (2000) 2566.

- 1
2
3
4
5
6
7
8
9
10
11
12
13
14
15
16
17
18
19
20
21
22
23
24
25
26
27
28
29
30
31
32
33
34
35
36
37
38
39
40
41
42
43
44
45
46
47
48
49
50
51
52
53
54
55
56
57
58
59
60
61
62
63
64
65
- 852 [38] M. Elimelech, C.R. O'Melia, *Langmuir* 6 (1990) 1153.
- 853 [39] N. Kallay, M. Colic, D.W. Fuerstenau, H.M. Jang, E. Matijevic, *Colloid Polym.*
854 *Sci.* 272 (1994) 554.
- 855 [40] R. Hogg, T.W. Healy, D.W. Fuerstenau, *Trans. Faraday Soc.* 62 (1966) 1638.
- 856 [41] N. Kallay, S. Zalac, *J. Colloid Interface Sci.* 253 (2002) 70.
- 857 [42] W. Zhang, J. Crittenden, K.G. Li, Y.S. Chen, *Environ. Sci. Technol.* 46 (2012)
858 7054.
- 859 [43] E.P. Honig, G.J. Roebersen, P.H. Wiersema, *J. Colloid Interface Sci.* 36 (1971)
860 97.
- 861 [44] R.J. Hunter, Academic Press, New York, 1981, 386p.
- 862 [45] H.C. Hamaker, *Physica* 4 (1937) 1058.
- 863 [46] G. Frens, Dissertation, Utrecht, 1968, 88p.
- 864 [47] G.M. Bell, S. Levine, L.N. McCartney, *J. Colloid Interface Sci.* 33 (1970) 335.
- 865 [48] D. Leckband, J. Israelachvili, *Q. Rev. Biophys.* 34 (2001) 105.
- 866 [49] J. Gregory, *J. Colloid Interface Sci.* 51 (1975) 44.
- 867 [50] S.L. Carnie, D.Y.C. Chan, J. Stankovich, *J. Colloid Interface Sci.* 165 (1994) 116.
- 868 [51] S. Bhattacharjee, M. Elimelech, M. Borkovec, *Croat. Chem. Acta* 71 (1998) 883.
- 869 [52] S. Bhattacharjee, A. Sharma, *Langmuir* 12 (1996) 5498.
- 870 [53] S. Bhattacharjee, M. Elimelech, *J. Colloid Interface Sci.* 193 (1997) 273.
- 871 [54] D.C. Henry, *Proc. R. Soc. Lond. A* 133 (1931) 106.
- 872 [55] J. Lyklema, M. Minor, *Colloids Surf. A: Physicochem. Eng. Asp.* 140 (1998) 33.
- 873 [56] D.C. Henry, *Trans. Faraday Soc.* 44 (1948) 1021.
- 874 [57] H. Ohshima, *J. Colloid Interface Sci.* 168 (1994) 269.
- 875 [58] E. Hückel, *Physikalische Zeitschrift* 25 (1924) 204.
- 876 [59] M. Von Smoluchowski, L. Graetz, Leipzig, 1921, 385p.

- 1
2
3
4
5
6
7
8
9
10
11
12
13
14
15
16
17
18
19
20
21
22
23
24
25
26
27
28
29
30
31
32
33
34
35
36
37
38
39
40
41
42
43
44
45
46
47
48
49
50
51
52
53
54
55
56
57
58
59
60
61
62
63
64
65
- 877 [60] A. Revil, P. Glover, *Geophys. Res. Lett.* (1998) 691.
- 878 [61] P.N. Sen, C. Scala, M.H. Cohen, *Geophysics* 46 (1981) 781.
- 879 [62] A. Revil, P.W.J. Glover, *Phys. Rev. B* 55 (1997) 1757.
- 880 [63] A. Revil, *J. Geophys. Res.-Sol. Ea.* 105 (2000) 16749.
- 881 [64] S.S. Dukhin, V.N. Shilov, Wiley & Sons Incorporated John, New York, 1974,
882 192p.
- 883 [65] D.L. Parkhurst, C.A.J. Appelo, U.S. Geological Survey Water-Resources
884 Investigations Report, 1999, 312p.
- 885 [66] M. Caceci, W.P. Cacheris, *Byte* 9 (1984) 340.
- 886 [67] L. Bergstrom, *Adv. Colloid Interface Sci.* 70 (1997) 125.
- 887 [68] T. Hiemstra, W.H. Van Riemsdijk, *J. Colloid Interface Sci.* 301 (2006) 1.
- 888 [69] H.C. Schwarzer, W. Peukert, *Chem. Eng. Sci.* 60 (2005) 11.
- 889 [70] S. Biggs, *KONA* 24 (2006) 41.
- 890 [71] B. Gilbert, G.P. Lu, C.S. Kim, *J. Colloid Interface Sci.* 313 (2007) 152.
- 891

892 **Table 1.** Optimized parameters of our aggregation kinetics model (constant effective
 893 interaction radius).

Parameters	DA	SEI
d_{\min} nm	3.4 ± 1	4 ± 1
A_H 10^{-20} J	5.89 ± 0.2	7.68 ± 0.2
a_i nm	16.12 ± 1	28.68 ± 1
R^2	0.63	1.48

894

895

896 **Table 2.** Optimized parameters of our aggregation kinetics model (variable effective
 897 interaction radius; distances are expressed in nm).

Parameters	DA	SEI	DA	SEI
d_{\min}	2.4±1	2.7±1	1.66	1.66
A_H 10^{-20} J	6.81±0.2	8.32±0.2	7.13±0.2	8.71±0.2
a_i (pH = 6.3)	31.80±1	65.44±1	33.71±1	67.87±1
a_i (pH = 6.7)	17.82±1	29.36±1	19.08±1	30.91±1
a_i (pH = 8.4)	8.99±1	12.35±1	5.76±1	7.97±1
R^2	0.11	0.13	0.17	0.23

898

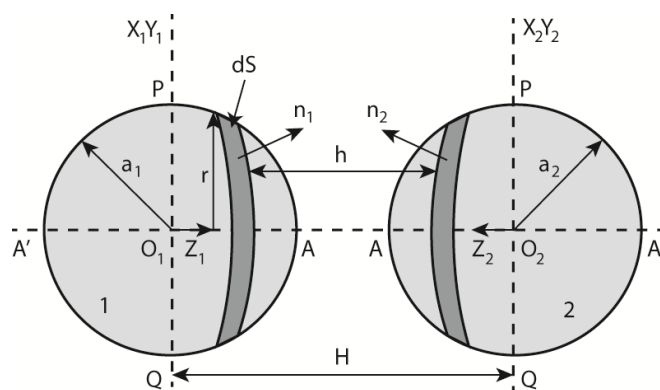


Fig. 1. Two interacting spherical particles with radii a_1 and a_2 . The centers of the spheres are origins of two body-fixed coordinate systems, with their z axes directly facing each other. The xy planes of these coordinate systems are parallel to each other (from Bhattacharjee et al. [51]).

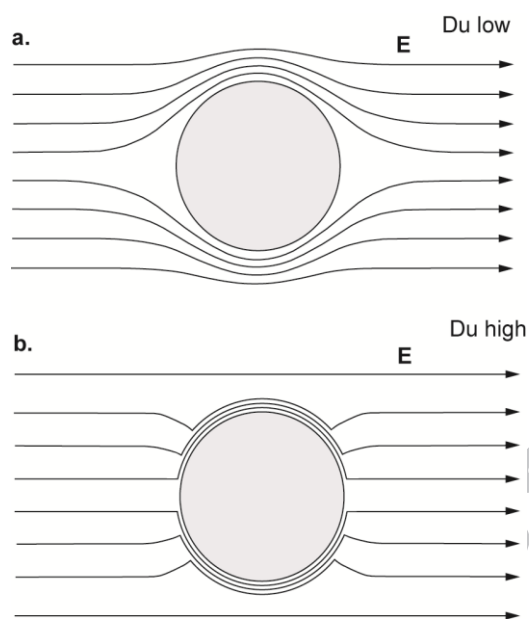


Fig. 2. Effect of the electrical double layer around the particle on the applied electrical field. Non-conducting particles (**a.**) and conducting particles (**b.**) (from Lyklema and Minor [55]). Du is the Dukhin number, which is defined as half the ratio of surface electrical conductivity to bulk electrical conductivity.

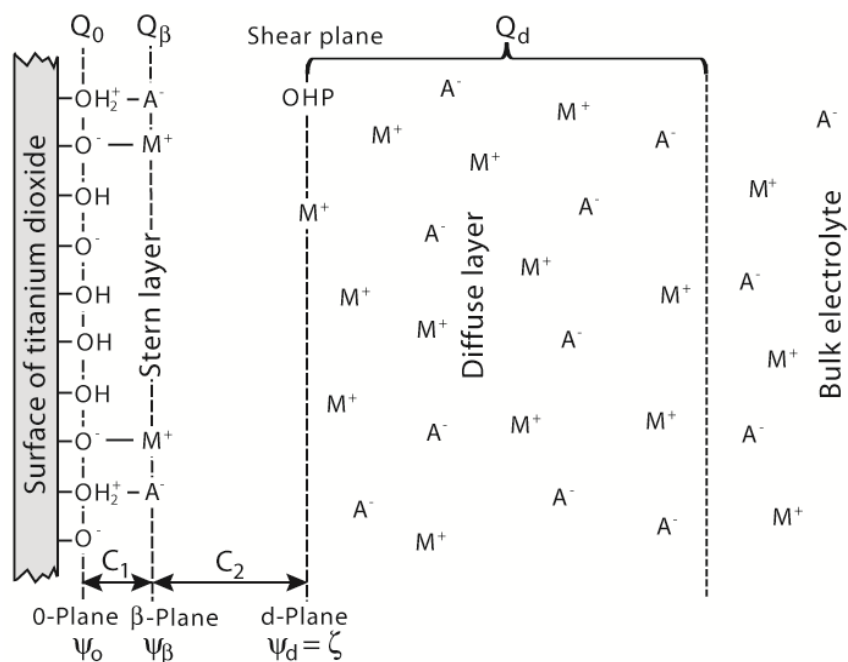


Fig. 3. The simplified sketch of the extended Stern model (ESM) of Leroy et al. [18]. M^+ are metal cations (e.g., Na^+ or K^+) and A^- are anions (e.g., Cl^-). OHP is the outer Helmholtz plane, which corresponds here to the shear plane where the zeta potential (ζ) is defined. Q is the surface charge density of the three different layers (mineral surface, Q_0 , Stern, Q_β , and diffuse layer, Q_d). C is the capacitance between the “0-plane” and the “ β -plane” (C_1), and between the “ β -plane” and the “ d -plane” (C_2).

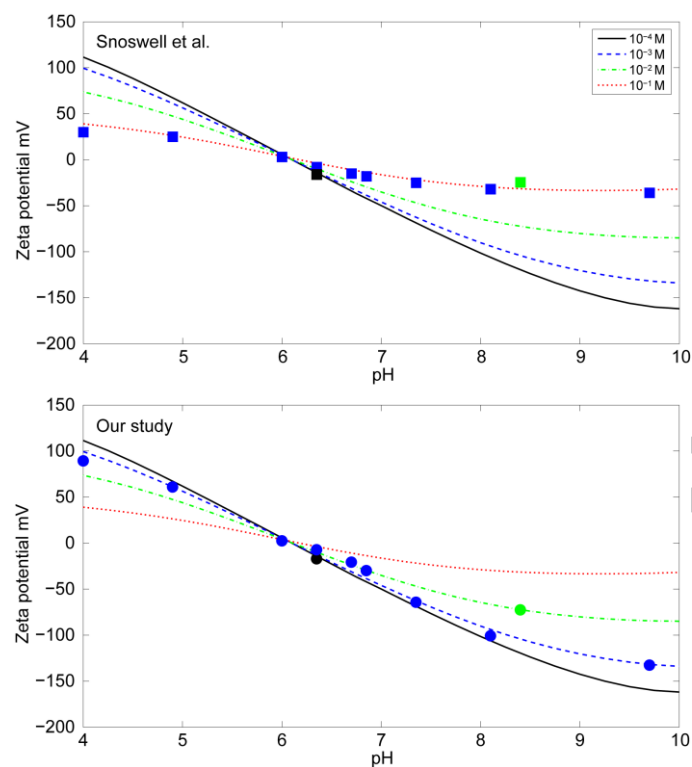


Fig. 4. “Observed” zeta potentials of pure TiO_2 NPs versus pH at 10^{-4} , 10^{-3} , and 10^{-2} M KCl from Snoswell et al. [22] (**a**; squares) and calculated using the approach of Leroy et al. [18] (**b**; circles). The curves are the ESM predictions assuming $\psi_d = \zeta$ [18].

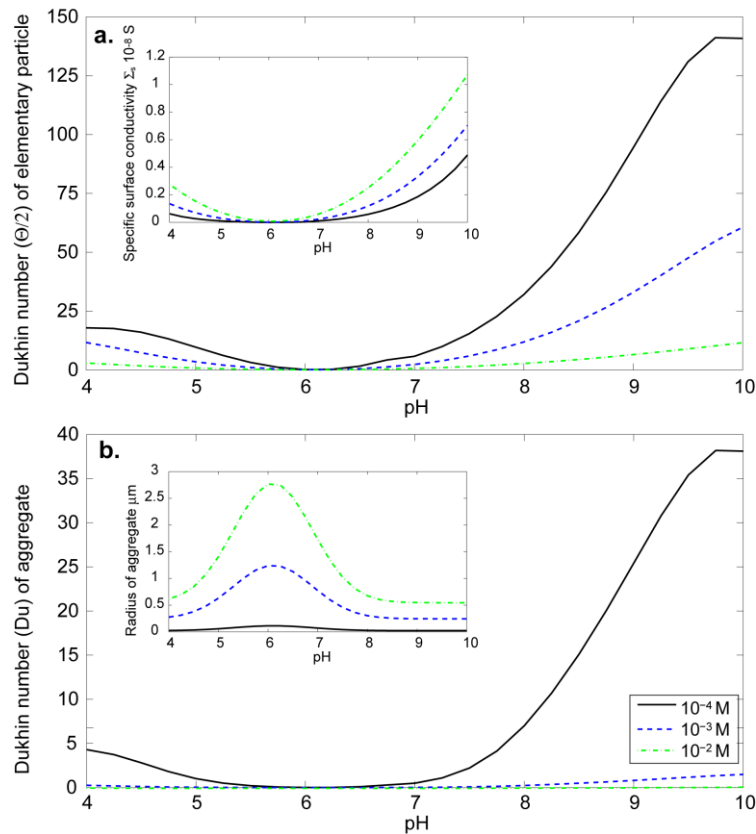


Fig. 5. The predicted Dukhin numbers of (a) an elementary NP and (b) an aggregate versus pH at 10^{-4} , 10^{-3} , and 10^{-2} M KCl. The mean radius of elementary NPs is equal to 6 nm ([22]), and the radius of the aggregate is optimized by decreasing the cost function

$$R^2 = \sum_{i=1}^L [\zeta_{\text{obs}}(i) - \psi_d(i)]^2$$

using the Simplex algorithm [66] (where L is the number of experimental values).

The intra-aggregate porosity is equal to 10 %.

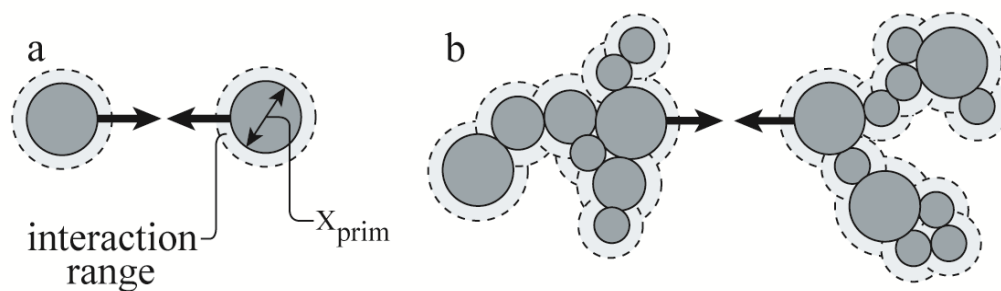


Fig. 6. The aggregation behavior of two nanoparticles (**a**) and of two aggregates (**b**) showing that stability is determined by the two nanoparticles involved if the range of interaction (defined by the thickness of the diffuse layer) is largely inferior to their size (from Schwarzer and Peukert [69]).

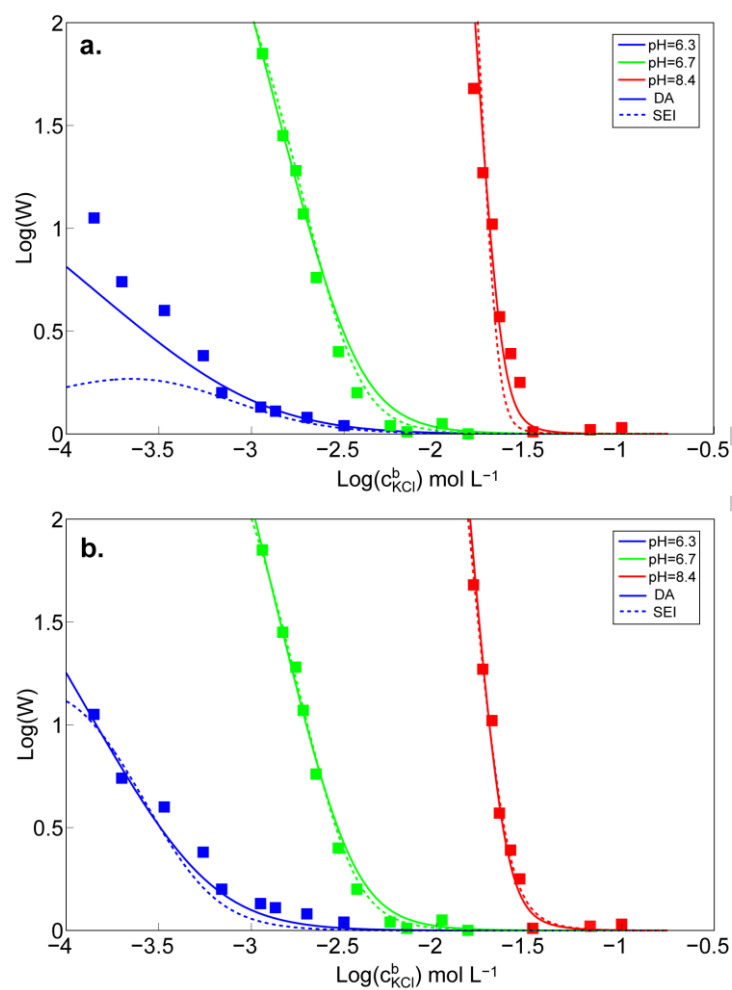


Fig. 7. Stability ratios versus salinity (KCl) (in log scale) at three different pH values (pH = 6.3, 6.7, and 8.4). Experimental data from Snoswell et al. [22] (squares) and model predictions with DA (solid lines) and SEI (dotted lines). Two cases are considered: the effective interaction radius is constant with pH (a) and the effective interaction radius varies with pH (b).

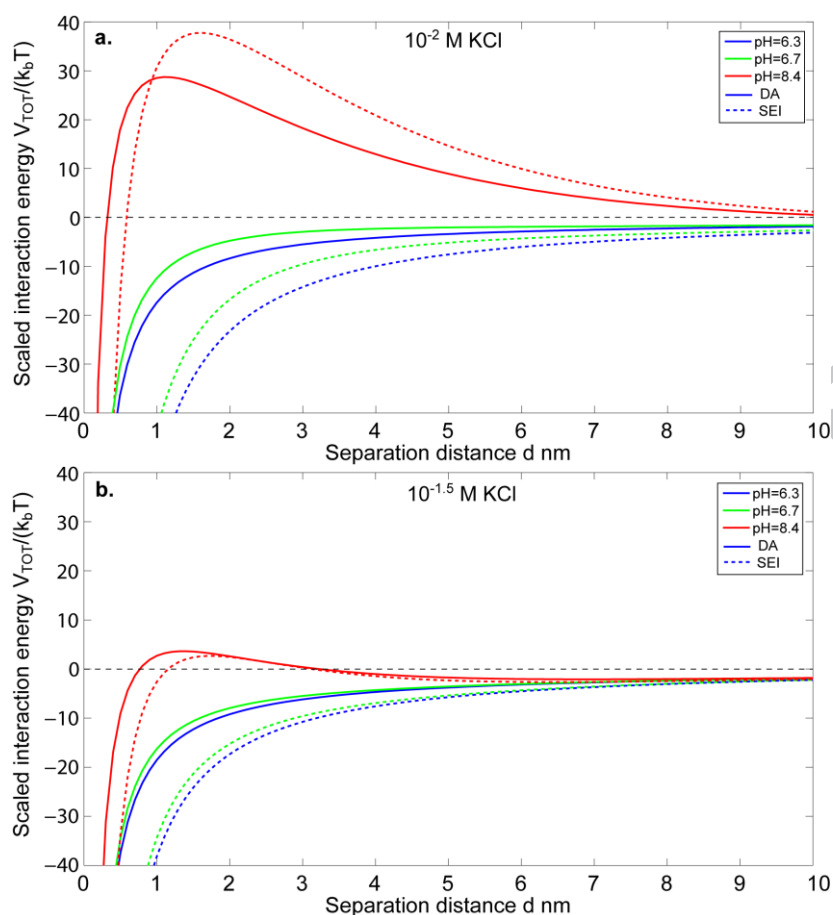


Fig. 8. Interaction energy profiles calculated by DA (solid lines) and SEI (dotted lines) at three different pH values (pH = 6.3, 6.7, and 8.4) and in the case of a constant effective interaction radius. **a.** Salinity of 10^{-2} M KCl. **b.** Salinity of $10^{-1.5}$ M KCl.

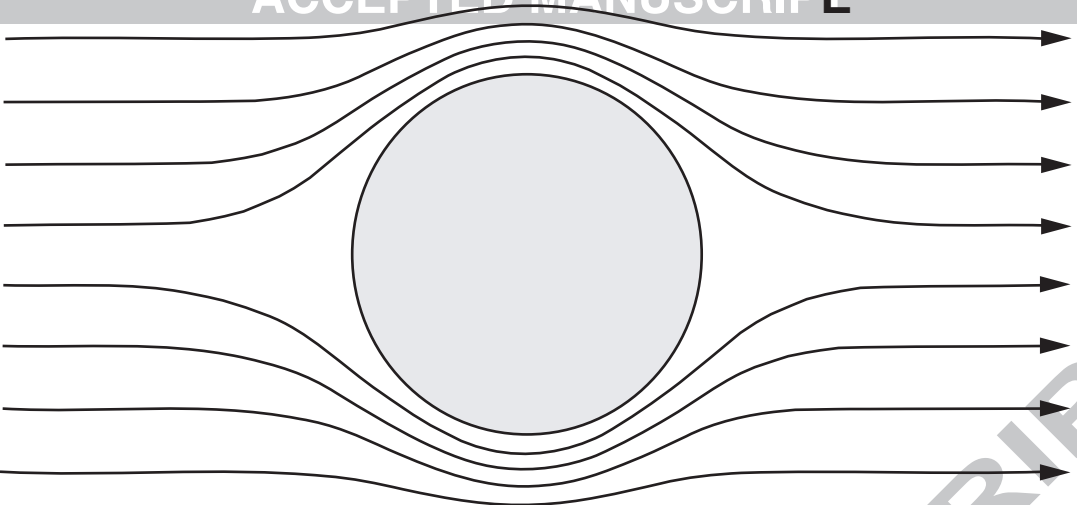
Table 1. Optimized parameters of our aggregation kinetics model (constant effective interaction radius).

Parameters	DA	SEI
d_{\min} nm	3.4 ± 1	4 ± 1
A_{H} 10^{-20} J	5.89 ± 0.2	7.68 ± 0.2
a_i nm	16.12 ± 1	28.68 ± 1
R^2	0.63	1.48

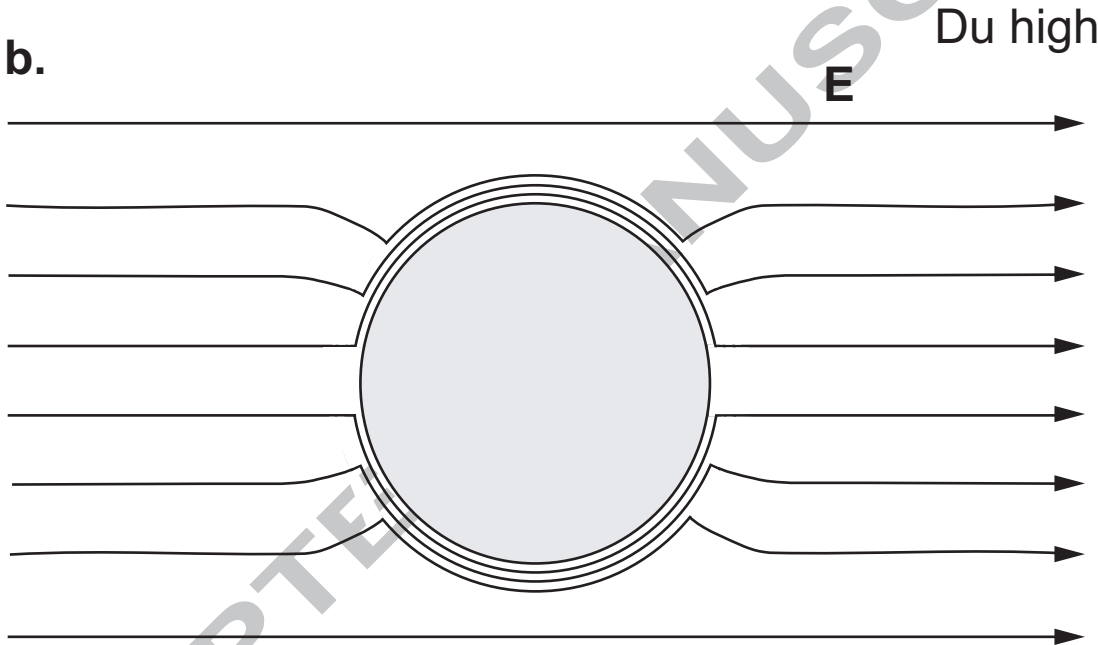
Table 2. Optimized parameters of our aggregation kinetics model (variable effective interaction radius; distances are expressed in nm).

Parameters	DA	SEI	DA	SEI
d_{\min}	2.4±1	2.7±1	1.66	1.66
A_H 10^{-20} J	6.81±0.2	8.32±0.2	7.13±0.2	8.71±0.2
a_i (pH = 6.3)	31.80±1	65.44±1	33.71±1	67.87±1
a_i (pH = 6.7)	17.82±1	29.36±1	19.08±1	30.91±1
a_i (pH = 8.4)	8.99±1	12.35±1	5.76±1	7.97±1
R^2	0.11	0.13	0.17	0.23

a.

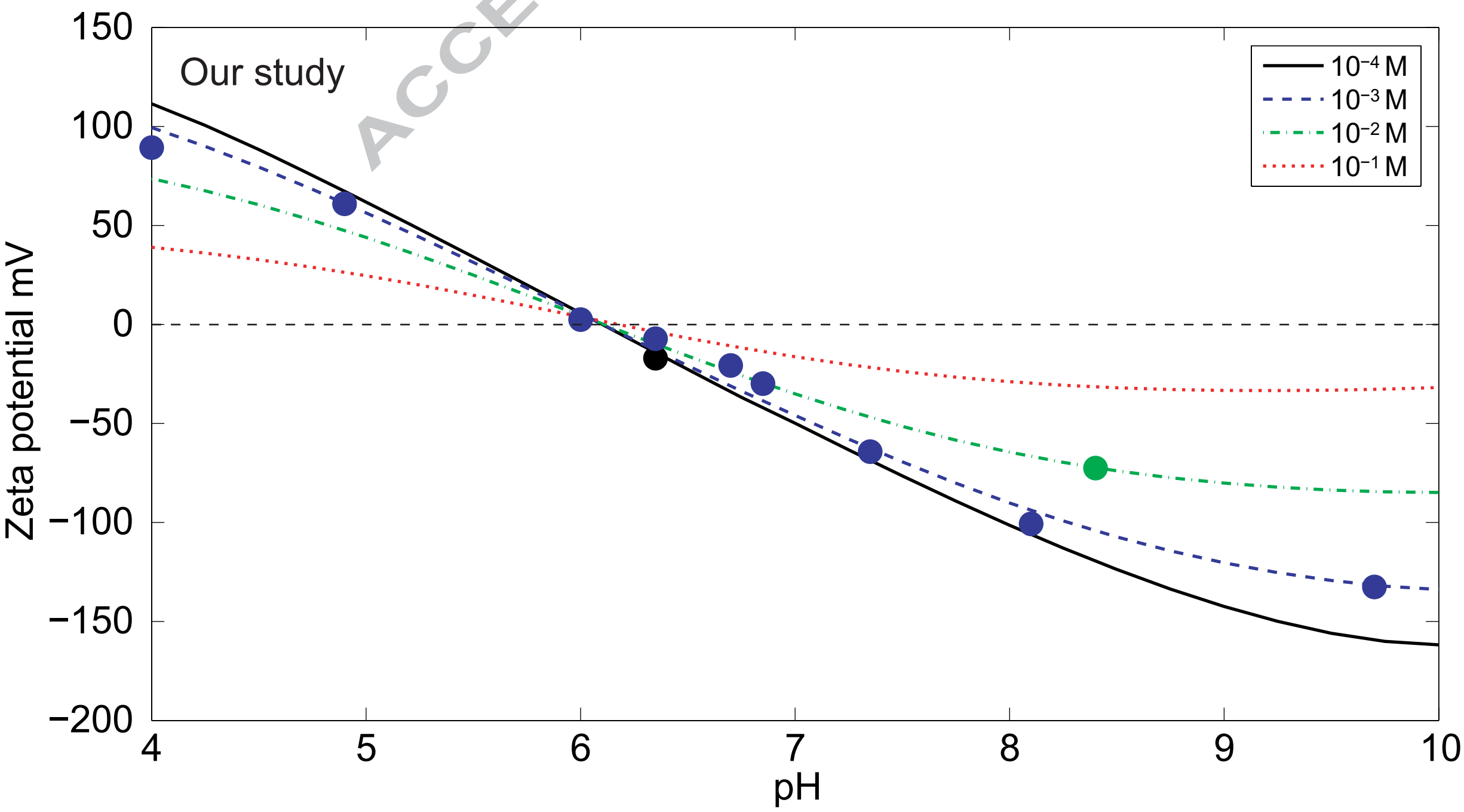
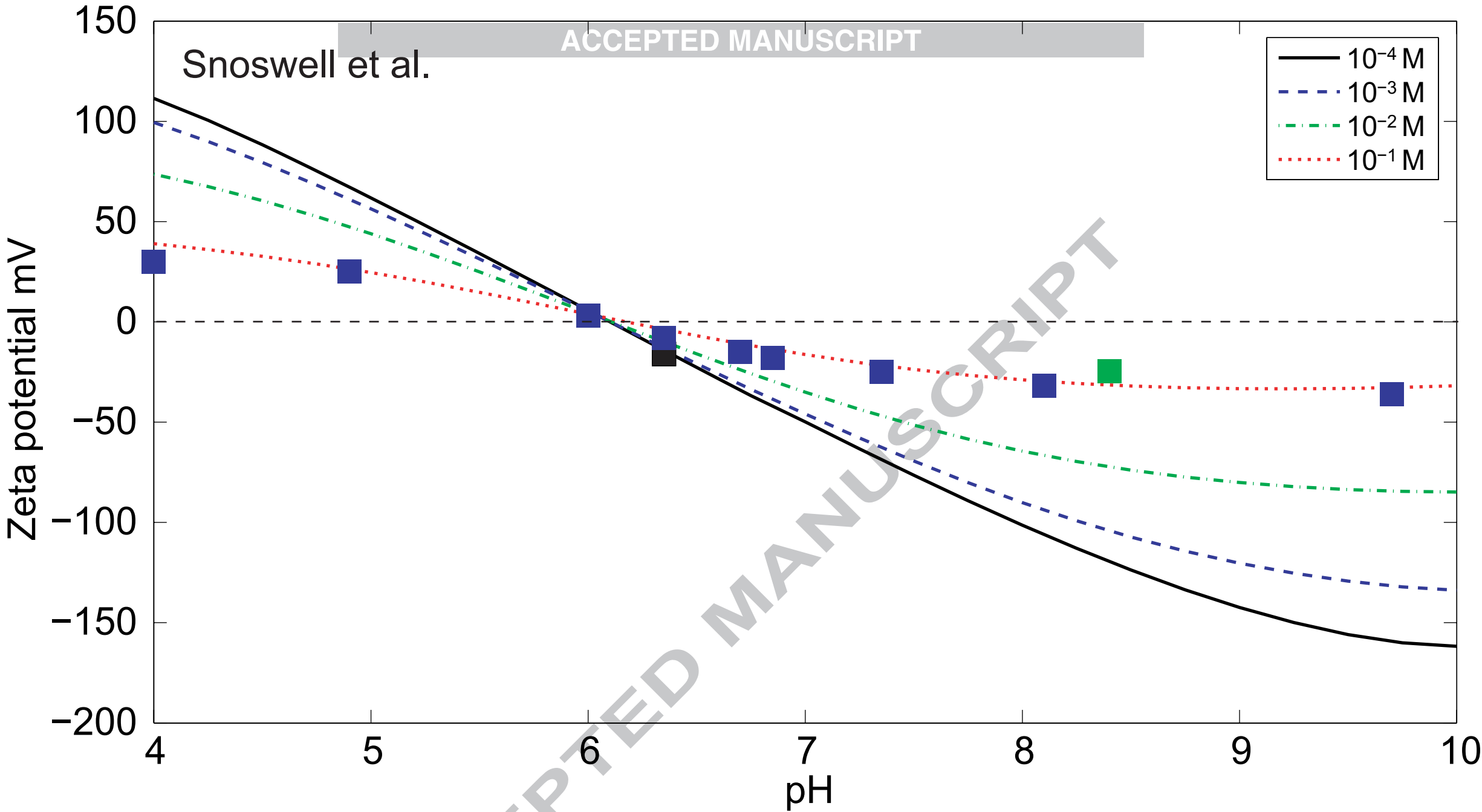


b.



Du high

E



Influence of surface conductivity on the apparent zeta potential of TiO₂ nanoparticles: application to the modeling of their aggregation kinetics

Izzeddine Sameut Bouhaik^{1,2}, Philippe Leroy^{1*}, Patrick Ollivier¹, Mohamed Azaroual¹, Lionel Mercury^{2,3}

¹ BRGM, ISTO UMR 7327, 45060 Orléans, France

² Université d'Orléans, ISTO UMR 7327, 45071 Orléans, France

³ CNRS/INSU, ISTO UMR 7327, 45071 Orléans, France

* Corresponding author and mailing address:

Philippe Leroy

BRGM

3 Avenue Claude Guillemin

45060 Orléans Cedex 2, France

E-mail: p.leroy@brgm.fr

Tel: +33 (0)2 38 64 39 73

Fax: +33 (0)2 38 64 37 19

The high surface conductivity of TiO₂ NPs decreases their electrophoretic mobility

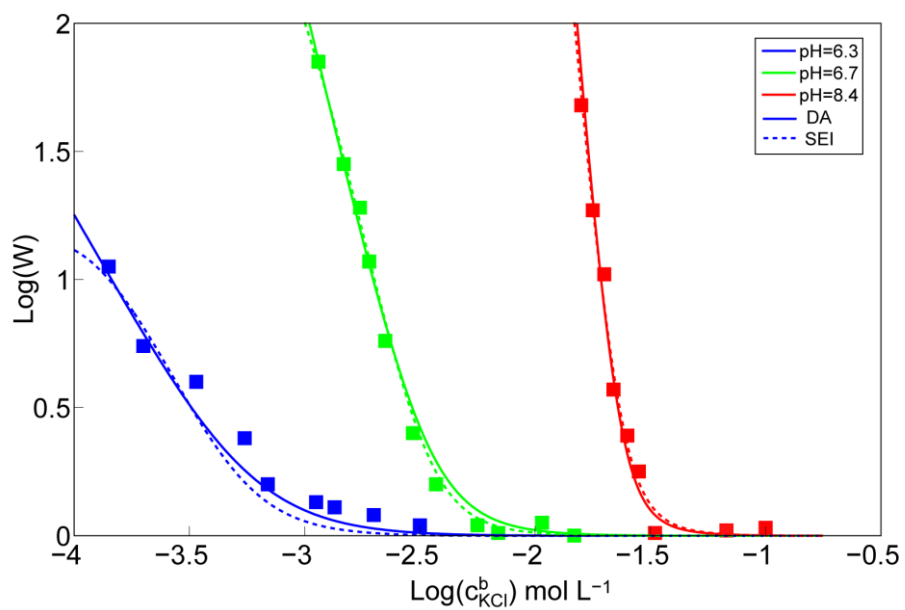
The zeta potential can be estimated directly from an extended Stern model

The true zeta potential can be twice that not corrected of surface conductivity

The effective interaction radius corresponds to that of primary particles

The aggregation kinetics of TiO₂ NPs can be predicted successfully by the DLVO theory

ACCEPTED MANUSCRIPT



Stability ratios of pure TiO₂ nanoparticles versus salinity (KCl) at three different pH values. Model predictions with Derjaguin approximation (solid lines) and surface element integration (dotted lines).